N71-33247

NASA TECHNICAL MEMORANDUM

NASA TM X-67896

NASA TM X-67896

DEFLECTION ANALYSIS OF DAMPED ROTORS WITH HARMONIC SUPPORT FORCES

by Richard H. Cavicchi
Lewis Research Center
Cleveland, Ohio
August 1971

ABSTRACT

A theoretical solution of the equations of motion is developed for damped rigid rotors with harmonic forces at the supports. Support deflection amplification and the phase angles between the displacements and the harmonic forces are computed. The harmonic forces represent the effects at the supports of unbalance forces whose planes of unbalance are assumed to have an equal distribution for the probability of their axial locations. Also, support stiffness and damping characteristics are assumed to be symmetrical. Under these conditions, which are representative of cylindrical roller bearings in rigid pedestals, a low-speed resonance appears when the center of gravity does not lie on the midplane. Other calculations show that even with a midplane center-of-gravity location, a low-speed resonance occurs for slender rotors but not for disks. Deflection amplification at low-speed resonances is generally smaller than at the major critical speed.

DEFLECTION ANALYSIS OF DAMPED ROTORS WITH HARMONIC SUPPORT FORCES

by Richard H. Cavicchi

Lewis Research Center

E-6504

SUMMARY

A theoretical steady-state analysis was performed to study damped vibrations of flexibly-mounted rigid rotors subjected to harmonic forces at the supports. The rotor-support system is mounted on a firm foundation. Viscous damping is assumed in which the viscous force is proportional to the rate of support displacement. Also, the support stiffness and damping characteristics are assumed to be symmetrical; symmetrical stiffness is a valid approximation for the characteristics of cylindrical roller bearings mounted on rigid pedestals. The harmonic forces are representative of the effects at the supports of unbalance forces. Thus, there is an equal distribution of the probability of the axial location of the planes of unbalance. A proportional relation is assumed between the force amplitudes at the two supports. The results of this analysis are calculated values for the support deflection amplifications and the phase angles between the displacement and the harmonic driving forces.

Seven illustrative cases are selected to display the results of the analysis graphically over a wide range of rotational speed. The parameters varied in these cases are damping, rotor shape (which is varied from a thin shape to a disk), center-of-gravity location, and force ratio at the supports.

The graphical results reveal that in addition to resonance at the major critical speed, a lower-frequency resonance occurs when the center of gravity is not located at the midplane. Other calculations show that even with the center of gravity at the midplane, a lower-frequency resonance occurs if the polar-to-diametral moment-of-inertia ratio is less than 0.7. Thus, disks should not experience the low-frequency resonance. Deflection amplification is generally greater at the major critical speed resonance than at the lower-frequency resonance; however, the low-frequency amplification may be greater for highly damped rotors.

Results from varying the center-of-gravity location suggest that there are certain locations that should be avoided in design because of potentially large deflection amplification.

INTRODUCTION

The problem of vibration effects in rotating machinery has been investigated for more than a century. Understanding of this problem has advanced considerably in recent years as the need for high-speed rotors has intensified the effort in rotor dynamics. Numerous investigators

have used various models, approaches, and conditions in this work. Among various aspects of this problem that have been studied are critical speeds, deflections, dynamic stability, transient effects, and the effects of acceleration.

The ability to predict and control rotor dynamics, as reflected by these aspects, is vitally important in the design of modern high-speed rotating machinery. Such machinery is frequently designed to operate at speeds above the rigid-body critical speeds. Thus, in startup and shutdown, rotors must pass safely through these critical-speed regimes. Usually, acceleration or deceleration is performed as rapidly as possible in order to avoid a damaging buildup of resonant amplitude. As improved analytical and design techniques are developed to predict and control critical speeds and resonant amplitudes, the designer will have greater freedom to design for operation near or even at critical speeds.

Reference 1 presents an analysis that identifies critical speeds for vibrations of undamped rotors on firm foundations. The critical speeds include major critical speed (precession frequency equal to rotor frequency) and nonsynchronous critical speeds (other speeds at which deflection amplification may occur). Yamamoto's analytical and experimental work, reported in reference 2, shows that bearing defects cause nonsynchronous critical speeds. In reference 3, Gunter inquires into the dynamic stability of rotor-bearing systems.

The analysis in reference 4 locates critical speeds for free vibrations of undamped rotors on flexible foundations. It studies the effects of variations in rotor speed, rotor and foundation shapes, and rotor-to-foundation spring-constant ratio. A comparison of the firm- and flexible-foundation results of references 1 and 4 appears in reference 5.

In reference 6, Gunter and DeChoudhury provide ALGOL computer programs to study steady-state effects of rotor unbalance, dynamic stability, and transient response. The linearized equations used in this reference contain cross-coupling stiffness and damping coefficients.

The present report extends the analytical work on rotors of reference 1 to include viscous damping and harmonic disturbing forces. It determines critical speeds, support deflections, and phase angles in response to harmonic equal and unequal forces at the supports. The harmonic forces at the supports represent the effects at the supports of unbalance forces that have an equal probability for axial location or magnitude. Another application of the harmonic forces in this report is to the magnetic forces in a turboalternator. Effects of this type of force on a rotor are studied in reference 7. Experimental values of cross-coupling coefficients are usually difficult to determine. The present report therefore uses a simplified version of the equations of motion that omits cross-coupling terms. The simplified analysis is used in this report to show trends resulting from varying damping, force ratio at supports, center-of-gravity location, and moment-of-inertia ratios. Seven combinations of parameters are used to illustrate the trends.

DESCRIPTION OF ROTOR-SUPPORT MODEL

Figure 1 is a sketch representing the support system of a rotor with damping. This study considers lateral motion (in the y- and z-directions) but no axial motion (x-direction). The symbols are defined in appendix A.

The support spring constant $k/2$ is assumed to have the same value for both supports in both the y- and z-directions. This is a good approximation for cylindrical roller bearings mounted in rigid pedestals. Likewise, a common value of damping factor $b/2$ is used at both supports in both directions. Static deflections are neglected; this would apply to conditions in space.

Harmonic Exciting Forces

Forced vibration due to the unbalance of eccentricity can be represented by a harmonic force acting at the center of gravity and a harmonic couple. The amplitudes of this force and couple are independent of time. These amplitudes are, however, functions of rotational speed which is independent of time in the steady-state solutions of this analysis.

For convenience in this study, the resultant force at the center of gravity is resolved into lateral components acting at the supports. The couple is replaced by the equivalent effects of the moments about the center of gravity of the force components at the supports.

The left support in figure 1 is designated as support 1 for identification and the right support is support 2. The force amplitude at support 2 is assumed to be proportional to the value at support 1. In the examples given in the report the proportionality factor r has been assigned values of 0, 1, and 2 to represent possible exciting force conditions due to unbalance.

Viscous damping at the supports is assumed in which the retarding force is taken to be proportional to the rate of displacement at the shaft supports.

Rotor Shape

Rotor configurations that vary from shapes as thin as pencils to the other extreme represented by disks are considered in this analysis. Shape is expressed in terms of the rotor polar moment of inertia I_p and its diametral moment of inertia I_D. The analysis is made nondimensional for generality; therefore, these two moments of inertia are expressed as

$$\pi_2 = I_D/M\ell^2 \tag{1}$$

and

$$\pi_3 = I_p/I_D \tag{2}$$

Both parameters have small values for slender shapes. For example, $\pi_3 = 0.0149$ for a rod whose length is 10 times its diameter. Its value for a thin disk is 2. The parameter π_2, called the disk effect, is zero for a concentrated mass and is infinite for a disk having all its mass distributed over a large radius.

Center-of-Gravity Location

Although the center of gravity is assumed to remain on the shaft centerline, its axial location is varied. In the examples, four typical values are specified for this location, from midplane to outboard quarter point, the last of which represents an overhung configuration.

ANALYSIS

Exciting Forces

The disturbing force components F_{y_1} and F_{z_1} in the model of figure 1 are assumed to be harmonic and represented by

$$F_{y_1} = F(\omega)\cos \omega t \tag{3}$$

and

$$F_{z_1} = F(\omega)\sin \omega t \tag{4}$$

acting at support number 1. The corresponding components at support 2 are assumed to be the multiples

$$F_{y_2} = r_y F_{y_1} \tag{5}$$

and

$$F_{z_2} = r_z F_{z_1} \tag{6}$$

The force amplitude $F(\omega)$ is assumed to be independent of time as discussed earlier. In particular, $F(\omega) = m\omega^2 e$ represents an unbalance force due to eccentricity e. On the other hand $F(\omega) =$ a constant represents the magnetic forces in a turboalternator as shown in reference 7.

Moments About Center of Gravity

The resulting moment about the y-axis through the center of gravity is

$$\mathcal{M}_y = -\ell_1 F_{z_1} + \ell_2 F_{z_2} \tag{7}$$

The moment about the z-axis is

$$\mathcal{M}_z = \ell_1 F_{y_1} - \ell_2 F_{y_2} \tag{8}$$

When equations (3) to (6) are used, the two moment equations become

$$\mathcal{M}_y = F(\ell_2 r_z - \ell_1)\sin \omega t \tag{9}$$

$$\mathcal{M}_z = -F(\ell_2 r_y - \ell_1)\cos \omega t \tag{10}$$

Equations of Motion

The following equations of motion are a mathematical approximation of the rotor-support model of this study.

$$\frac{\ell_2 M\ddot{y}_1}{\ell} + \frac{\ell_1 M\ddot{y}_2}{\ell} + \frac{b}{2}(\dot{y}_1 + \dot{y}_2) + \frac{k}{2}(y_1 + y_2) = F(\omega)(1 + r_y)\cos \omega t \tag{11}$$

$$\frac{\ell_2 M\ddot{z}_1}{\ell} + \frac{\ell_1 M\ddot{z}_2}{\ell} + \frac{b}{2}(\dot{z}_1 + \dot{z}_2) + \frac{k}{2}(z_1 + z_2) = F(\omega)(1 + r_z)\sin \omega t \tag{12}$$

$$\frac{I_p}{\ell}(\dot{y}_2 - \dot{y}_1) - \frac{I_D}{\ell}(\ddot{z}_2 - \ddot{z}_1) - \frac{b}{2}\ell_2\dot{z}_2 + \frac{b}{2}\ell_1\dot{z}_1 - \frac{k}{2}\ell_2 z_2 + \frac{k}{2}\ell_1 z_1 = F(\omega)(\ell_2 r_z - \ell_1)\sin \omega t \tag{13}$$

$$\frac{I_p}{\ell}(\dot{z}_2 - \dot{z}_1) + \frac{I_D}{\ell}(\ddot{y}_2 - \ddot{y}_1) + \frac{b}{2}\ell_2\dot{y}_2 - \frac{b}{2}\ell_1\dot{y}_1 + \frac{k}{2}\ell_2 y_2 - \frac{k}{2}\ell_1 y_1 = -F(\omega)(\ell_2 r_y - \ell_1)\cos \omega t \tag{14}$$

Laplace Transforms

It is convenient to take the Laplace transforms of the equations of motion. The following development assumes that the support displacements and derivatives at time zero are zero.

With the following type of notation for a Laplace transform

$$\mathcal{L}[y(t)] = Y(s) = Y \tag{15}$$

and zero initial conditions, the equations of motion can be expressed as

$$Y_1\left(\frac{M\ell_2}{\ell}s^2 + \frac{b}{2}s + \frac{k}{2}\right) + Y_2\left(\frac{M\ell_1}{\ell}s^2 + \frac{b}{2}s + \frac{k}{2}\right) = \frac{s(r_y + 1)F(\omega)}{s^2 + \omega^2} \tag{16}$$

$$Z_1\left(\frac{M\ell_2}{\ell}s^2 + \frac{b}{2}s + \frac{k}{2}\right) + Z_2\left(\frac{M\ell_1}{\ell}s^2 + \frac{b}{2}s + \frac{k}{2}\right) = \frac{\omega(r_z + 1)F(\omega)}{s^2 + \omega^2} \tag{17}$$

$$-Y_1\left(\frac{I_p}{\ell}s\right) + Y_2\left(\frac{I_p}{\ell}s\right) + Z_1\left(\frac{I_D}{\ell}s^2 + \frac{b\ell_1}{2}s + \frac{k\ell_1}{2}\right) - Z_2\left(\frac{I_D}{\ell}s^2 + \frac{b\ell_2}{2}s + \frac{k\ell_2}{2}\right)$$
$$= \frac{\omega(\ell_2 r_z - \ell_1)F(\omega)}{s^2 + \omega^2} \tag{18}$$

$$-Y_1\left(\frac{I_D}{\ell}s^2 + \frac{b\ell_1}{2}s + \frac{k\ell_1}{2}\right) + Y_2\left(\frac{I_D}{\ell}s^2 + \frac{b\ell_2}{2}s + \frac{k\ell_2}{2}\right) - Z_1\left(\frac{I_p}{\ell}s\right) + Z_2\left(\frac{I_p}{\ell}s\right)$$
$$= \frac{-s(\ell_2 r_y - \ell_1)F(\omega)}{s^2 + \omega^2} \tag{19}$$

The coefficients of the Laplace variables are constants A_1, A_2, B_1, B_2, and C as defined in the symbols list. Use of these constants in equations (16) to (19) yields

$$A_2Y_1 + A_1Y_2 = \frac{s(r_y + 1)F(\omega)}{s^2 + \omega^2} \tag{20}$$

$$A_2Z_1 + A_1Z_2 = \frac{\omega(r_z + 1)F(\omega)}{s^2 + \omega^2} \tag{21}$$

$$-CY_1 + CY_2 + B_1Z_1 - B_2Z_2 = \frac{\omega(\ell_2 r_z - \ell_1)F(\omega)}{s^2 + \omega^2} \tag{22}$$

$$-B_1Y_1 + B_2Y_2 - CZ_1 + CZ_2 = \frac{-s(\ell_2 r_y - \ell_1)F(\omega)}{s^2 + \omega^2} \tag{23}$$

Deflection Solutions

The object of this analysis is to solve equations (20) to (23) for the deflections represented by Y_1 and Y_2 at each support. Due to symmetry, the deflections Z_1 and Z_2 differ from Y_1 and Y_2 only by 90° in phase angles; therefore, no solutions will be developed for Z_1 and Z_2. The solutions for Y_1 and Y_2 are given by

$$Y_1 = \left(\frac{F(\omega)}{s^2 + \omega^2}\right)\frac{N_1}{D} \tag{24}$$

and

$$Y_2 = \left(\frac{F(\omega)}{s^2 + \omega^2}\right)\frac{N_2}{D} \tag{25}$$

where

$$N_1 = \begin{vmatrix} (r_y + 1)s & A_1 & 0 & 0 \\ (r_z + 1)\omega & 0 & A_2 & A_1 \\ (\ell_2 r_z - \ell_1)\omega & C & B_1 & -B_2 \\ -(\ell_2 r_y - \ell_1)s & B_2 & -C & C \end{vmatrix} \tag{26}$$

$$N_2 = \begin{vmatrix} A_2 & (r_y + 1)s & 0 & 0 \\ 0 & (r_z + 1)\omega & A_2 & A_1 \\ -C & (\ell_2 r_z - \ell_1)\omega & B_1 & -B_2 \\ -B_1 & -(\ell_2 r_y - \ell_1)s & -C & C \end{vmatrix} \tag{27}$$

$$D = \begin{vmatrix} A_2 & A_1 & 0 & 0 \\ 0 & 0 & A_2 & A_1 \\ -C & C & B_1 & -B_2 \\ -B_1 & B_2 & -C & C \end{vmatrix} \tag{28}$$

Expressions for N_1, N_2, and D obtained from expanding the determinants in equations (26) to (28) are given in appendix B.

All variables are made dimensionless in this analysis and are summarized here for reference.

$$\pi_1 = \frac{s}{\sqrt{k/M}} \tag{29}$$

$$\pi_2 = \frac{I_D}{M\ell^2} \tag{1}$$

$$\pi_3 = \frac{I_p}{I_D} \tag{2}$$

$$\pi_4 = \frac{\omega}{\sqrt{k/M}} \tag{30}$$

$$\pi_{10} = \frac{b}{\sqrt{kM}} \tag{31}$$

$$L_1 = \frac{\ell_1}{\ell} \tag{32}$$

$$L_2 = \frac{\ell_2}{\ell} \tag{33}$$

Deflection Amplitude and Phase Angle

This report studies the frequency response to a sinusoidal input. Mathematically, this is achieved by setting $s = i$. In dimensionless form, this is

$$\pi_1 = i\pi_4 \tag{34}$$

Then

$$\frac{\frac{Y}{F(\omega)}}{k} = \frac{a + ic}{b + ih} \tag{35}$$

from which the magnitude is

$$\left| \frac{\frac{Y}{F(\omega)}}{k} \right| = \sqrt{\frac{a^2 + c^2}{g^2 + h^2}} \tag{36}$$

and the phase angle between the deflection and exciting force is

$$\theta = \tan^{-1}\left(\frac{cg - ah}{ag + ch}\right) \tag{37}$$

Detailed expressions for a, c, g, and h are presented in appendix B.

Normalized Deflection

The ratio in equation (36) is normalized by dividing by its value at zero rotational speed (when $\pi_4 = 0$) which represents the deflection at zero exciting frequency or large stiffness; therefore, equation (36) is expressed by the amplification factor

$$\mu = \frac{\left|\frac{Y_1}{F(\omega)/k}\right|}{\left|\frac{Y_1}{F(\omega)/k}\right|_{\pi_4=0}} = \frac{\sqrt{\frac{a^2 + c^2}{g^2 + h^2}}}{\sqrt{\left(\frac{a^2 + c^2}{g^2 + h^2}\right)_{\pi_4=0}}} \tag{38}$$

The normalizing factors are derived in appendix B. Then, by equations (B16) and (B17), equation (36) becomes

$$\mu_1 = \frac{\left|\frac{Y_1}{F(\omega)/k}\right|}{\left|\frac{Y_1}{F(\omega)/k}\right|_{\pi_4=0}} = \frac{\sqrt{\frac{a_{1r}^2 + c_{1r}^2}{g^2 + h^2}}}{2[L_2(2r + 1) - L_1]} \tag{39}$$

for support 1. The corresponding expression for support 2 is

$$\mu_2 = \frac{\left|\frac{Y_2}{F(\omega)/k}\right|}{\left|\frac{Y_2}{F(\omega)/k}\right|_{\pi_4=0}} = \frac{\sqrt{\frac{a_{2r}^2 + c_{2r}^2}{g^2 + h^2}}}{2[r(L_2 - L_1) - 2L_1]} \tag{40}$$

CATALOG OF RESULTS

Parameter Selections

An abundance of parameter combinations is possible for making calculations in this analysis. Seven particular combinations were chosen to display the effects of parameter variations. The intention was to provide meaningful results with minimum data production.

The seven parameter combinations selected are tabulated in table I.

Data Plots

For each of the seven cases of table I, calculations were made for the amplification factor μ (eqs. (39) and (40)) and phase angle θ (eq. (37)) for both supports. Data plots were made in which μ and θ are each plotted against rotor rotational parameter π_4. Each point on the data plots represents a steady-state point.

A negative angle represents a phase lag between the driving force and the support displacement.

Case 1. - The case 1 data plots in figure 2 are typical of the frequency response of classic second-order systems presented in textbooks. Perfect symmetry is assumed for case 1. That is, the center of gravity is at the midplane ($L_1 = L_2 = 0.5$) and both supports are subjected to forces of the same amplitude ($r_y = r_z = r = 1$). Figure 2(a) shows the effect of damping parameter π_{10} on amplification factor and figure 2(b), on phase angle.

The amplification factor in figure 2(a) is very sensitive to the amount of damping in the region about $\pi_4 = 1$. This, of course, is the condition for which the rotational frequency equals the natural frequency. Because the amplification factor becomes infinite in an undamped system at $\pi_4 = 1$, it is also referred to as the major critical speed. Farther removed from the condition of $\pi_4 = 1$, the effect of damping on amplification factor is minor.

Figure 2(a) also shows the typical effect that the resonance peaks occur at gradually lower rotational speeds as damping is increased. No peak at all is reached for values of π_{10} greater than a value of about 1.2.

Forced vibrations with viscous damping are harmonic and have the same frequency as the driving force. The lateral support deflections, however, are out of phase with the driving force. The phase lag is presented in figure 2(b) as a function of damping and rotational speed parameter. At the major critical speed, all systems show a phase lag of 90° irrespective of the amount of damping. Below this value, highly damped systems have the greatest phase lags. Above $\pi_4 = 1$, the opposite is true. At rotational speeds near the major critical, the phase angle is extremely sensitive to rotational speed for lightly damped rotors.

Figure 2 shows that μ approaches 1 and θ approaches zero for all values of damping as the rotational speed approaches zero. Thus, at low rotational speeds the deflection is the same as though the force were applied statically. Also, at high rotational speeds the phase lag for all values of damping parameter approaches 180°.

Case 2. - The plots in figure 3 show the effect of damping for the extreme condition in which support 2 experiences no exciting force ($r = 0$). The ordinate in figure 3(a) is given as a deflection-speed parameter $\left(\frac{Y_1}{F(\omega)/k}\right)\left(\frac{\pi_1^2 + \pi_4^2}{\pi_1^2}\right)$. A normalizing factor at zero rotational speed is not used for support 1 for case 2 because it is zero for $r = 0$ and $L_1 = L_2 = 0.5$ (see eq. (B16)). All other deflection parameter plots in this report are normalized except for figure 3(a). Figure 3(b) shows the amplification factor for support 2. Solutions for equations (20) to (23) for Z_1 and Z_2 were obtained, although not presented in this report. They reveal zero deflection in the z-direction at support 1 at zero speed when r is zero.

Equations (B18) and (B19) relate r and the center-of-gravity location for zero rotational speed and zero deflection at each support. When the center of gravity is at the midplane ($L_1 = L_2$), equation (B18) shows that $r = 0$ for zero deflection at support 1. But, according to equation (B19) there is no center of gravity location for which $r = 0$ when the deflection at support 2 is zero at zero rotational speed.

Figure 3(b) shows that there is no deflection amplification for support 2 when the damping parameter π_{10} is above about 0.6. By comparison, the critical damping parameter is 2.0 for free vibrations with midplane center of gravity. Critical damping may be defined as the value for which maximum amplification factor is 1.

In the phase angle plots of figures 3(c) and (d) all curves do not pass through 90° at $\pi_4 = 1$ as occurs for case 1. This results from the lack of symmetry of the exciting force.

Case 3. - In case 3, support 2 is subjected to twice the force of support 1 ($r = 2$). Figure 4 presents the curves for this case. Figure 4(a) shows a critical value of π_{10} at a little greater than 0.8 for support 1. The corresponding value for support 2 is 2.2 (fig. 4(b)).

In the phase-angle plots of figures 4(c) and (d), the $\pi_4 = 1$ crossings are more closely bunched than for case 2. Otherwise, the curves in figures 4(c) and (d) are similar to those in figures 3(c) and (d).

Case 4. - Figure 5 presents plots that show the effect of center-of-gravity location. When the rotor center of gravity is located away from the midplane, an additional set of resonances appears. This set of resonances is also influenced by the support stiffness and damping characteristics, which are assumed to be symmetrical in this analysis. The result is that with a distribution of equal probability of the axial location of the planes of unbalance, the probability of exciting a low-frequency resonance increases if the center of gravity is not located at the midplane. The rotor rigid body cylindrical and conical modes

are coupled together when the center of gravity does not lie on the midplane.

Figures 5(a) and (b) show a resonance peak occurring at a rotational speed below the major critical for each curve except the $L_1 = 0.5$ curve. The low frequency resonances are much smaller in both amplification and magnitude than those at the major critical speed. This means that a given amount of damping is more effective in displacement attenuation at the low-speed resonance.

Figures 5(a) and (b) show that as the center of gravity is located progressively farther from the midplane, the resonance peaks occur at lower rotational speeds. This observation is true for both the low- and high-frequency sets.

A conclusion from figures 5(a) and (b) is that even though additional resonances may occur when the center of gravity location is varied, the more severe deflection amplification occurs at the major critical speed.

Comparison of figures 5(a) and (b) reveals that at support 1, maximum deflection amplification occurs when the center of gravity lies at the quarter point ($L_1 = 0.75$). At support 2 the worst condition occurs when the center of gravity is at the midplane. Furthermore, greater amplifications occur at support 1 than at support 2.

Case 5. - In case 5 the center of gravity is located at the support subjected to the larger driving force (support 2). The damping parameter varies for this case which is presented in figure 6. The curves for $\pi_{10} = 0.1$ are repeated from figure 5. The two sets of resonance peaks are well defined. At both supports, the highest resonance peak of the low-frequency set occurs with a damping parameter of 0.5. Figure 6(a) shows no low-frequency resonance peak at zero damping. Instead, there is an antiresonance or minimum amplification. At support 2 with zero damping there is no resonance or antiresonance among the low-frequency set. On the other hand, the low frequency peaks in figure 6(b) are higher for $\pi_{10} \geq \sqrt{2}$ than the high frequency peaks in figure 6(a).

The critical value of π_{10} for support 1 is about three for the low-frequency set as shown in figure 6(a) and 1.8 for the high-frequency set. At support 2, figure 6(b), the corresponding values for π_{10} are 2.8 and 0.6.

Comparison of figures 6(a) and (b) suggests that deflection amplification is more severe at support 1 than at support 2 when the center of gravity and the larger force are at support 2.

Case 6. - The results for case 6 appear in figure 7. This case presents the effect of the polar-to-diametral moment-of-inertia ratio π_3 on deflection amplification. At both supports the high frequency peaks all occur at $\pi_4 = 1$. In figures 7(a) and (b), no low-frequency peaks

occur for values of π_3 greater than 1. Therefore, disks ($\pi_3 = 2$) experience large deflection amplification at only the major critical speed whereas slender shapes have two resonant speeds. The value of $\pi_3 = 0$ is fictitious and merely sets a lower boundary to the calculations. The curves representing $\pi_3 = 1$ depart from the usual pattern at high rotational speeds.

The phase angle plots in figures 7(c) and (d) show all curves passing through 90° at $\pi_4 = 1$. This results because of the low value of the damping parameter ($\pi_{10} = 0.1$). The curves would not all pass through the 90° point at higher values of damping parameter as figures 4(c) and (d) imply.

Comparison of figures 7(a) and (c) shows that the phase-lag peaks of figure 7(c) occur at rotational speeds between the low-frequency resonances and the antiresonances of figure 7(a). This is also true for support 2 (figs. 7(b) and (d)).

Case 7. - Figure 8 presents the variation of the disk effect over a range from zero to 10. No additional resonances occur at either support. It should be realized that the value of π_3 used in figure 9 is 2. Figure 7 has shown that no low-frequency resonances occur when π_3 is one or greater; therefore, curves drawn for case 7 with π_3 values of 0.5 and lower may be expected to show low-frequency resonance peaks. But, the result of figure 8 is that varying the disk effect π_2 does not result in an additional resonance peak. The $\pi_2 = 0$ curve has no physical significance.

All the phase-angle curves for both bearings pass through 90° at the major critical speed in figures 8(c) and (d).

INTERPRETATION OF RESULTS

Cross plots were made of some of the amplification curves to aid in interpreting effects of the parameters varied. All amplification factors discussed in this section are peak amplification factors. They were read at the appropriate peak.

Damping

Figure 9 presents peak amplification factor as a function of damping parameter. Curves are shown for both supports. Cases 1, 2, and 3 are represented in figure 9(a) and case 5 results are in figure 9(b).

Center of gravity at midplane. - The center of gravity in figure 9(a) is located at the midplane. In this figure it is immediately apparent that all curves have the same slope on the logarithmic plot. They can all be represented by an expression of the form

$$\mu\pi_{10} = \text{constant} \qquad \mu > 1$$

which is linear on a logarithmic plot. The condition $\mu = 1$ corresponds to critical damping.

In figure 9(a), the line for $r = 1$ coincides with the support 1 line for $r = 0$ as long as $\mu > 1$. The $r = 1$ line, of course, is drawn for $Y_1/F(\omega)/k$; whereas the $r = 0$ line represents the normalized factor μ.

In a comparison of the dashed set of lines ($r = 0$) with the solid set ($r = 2$) in figure 9(a), it is evident that the amplification factor for both supports increases as the force ratio r is increased.

When $r = 0$, support 1 experiences greater amplification than support 2. The opposite is true when $r = 2$.

Center of gravity at support 2. - The center of gravity is located at support 2 for the model of figure 9(b). Figure 5 has shown that an additional set of resonance peaks occurs when the center of gravity is displaced from the midplane location. The low-frequency set is dashed in figure 9(b) and the high-frequency set is solid.

The high-frequency set shown in figure 9(b) has slopes essentially parallel to the lines in figure 9(a).

Support 1 is subjected to greater amplification than support 2, in figure 9(b), for both resonance sets. In figure 9(a) for $r = 2$, the opposite was observed.

Comparison of the dashed and solid curves in figure 9(b) shows that for highly damped rotors, the low-frequency amplification exceeds that of the high-frequency set. In all such cases, however, the amplification factor is less than 2.

The low-frequency set of curves in figure 9(b) reaches a peak at a damping factor of about 0.4. This implies that the amplification decreases for the low-frequency set as damping factor is decreased below 0.4. This circumstance is of no practical advantage, however, because of the large increase in amplification of the high frequency set.

Center-of-Gravity Location

Figure 10 presents the effect of center-of-gravity location on peak amplification factor as determined for case 4. Two sets of resonances appear in this figure for each support.

It is appropriate here to discuss the relative magnitudes of the curves for the two bearings at a given center-of-gravity location. Over

most of the range shown, the amplification factor for support 1 exceeds that of support 2 despite the fact that support 2 experience twice the force of support 1. This is not a paradox as can be seen by noting equations (B16) and (B17). For all values of L_1 and L_2 except when they are equal, the magnitude given by equation (B17) exceeds that of equation (B16); therefore, the normalizing factor used in calculating μ for support 2 exceeds that for support 1. Thus, although the actual deflection at support 2 is greater than that at support 1, its amplification factor μ is less.

The most important information given by figure 10 is that there are certain center-of-gravity locations that should be avoided in order to prevent large deflection amplification. For the conditions of case 4, locations given by L_1 in the vicinity of 0.83 should be avoided. Figure 10 shows peak amplification factors at support 1 at this location for both the low- and high-frequency resonances. Support 2 peaks occur at $L_1 = 0.6$ for both resonance sets so these locations should also be avoided. Calculations were made at very small increments in L_1 in order to define the location of these peaks accurately. The location of the peaks would be different for other parameter combinations, of course.

The amplification factor for support 1 exceeds that for support 2 over most of the center-of-gravity range studied. Below about 0.61 and above about 1.2 for L_1, the support 2 amplification is greater. The location at which the amplification factor of the high-frequency resonance set is the same for both supports is very close to the peak for support 2.

Polar-to-Diametral Moment of Inertia Ratio

Figure 11 presents the effect of polar-to-diametral moment-of-inertia ratio π_3 on amplification factor under the conditions of case 6. The most prominent aspect of figure 11 is the small effect that π_3 has on amplification factor of the high-frequency set.

For the low-frequency resonance set, in general, amplification factor decreases as π_3 increases. Above about 0.65 for π_3, no low-frequency set exists.

Over most of the range in figure 11, the amplification factor at support 2 is twice that at support 1.

Support Force Ratio

The effect of support force ratio r on amplification factor appears in figure 12. Damping parameter values of 0.1, 0.2, 0.5, 0.8, and 1 are used in this figure. Cases 1, 2, and 3 were used in producing figure 13.

At support 2, represented by dashed curves, the amplification factor increases approximately linearly with r. The support 1 curves decrease with increasing values of r. At $r = 1$ both supports experience the same amplification due to symmetry. As r approaches zero, the support 1 amplification approaches infinity, as verified by the fact that equation (B16) yields zero. The zero magnitude of equation (B16) occurs only when $L_1 = L_2$, of course. At $r = 0$, the amplification factor at support 2 remains finite (see eq. (B17)).

The reason that the amplification factor for support 1 is greater than that for support 2 is explained by the relative magnitudes of equations (B16) and (B17). Although the amplification factor for support 1 is approaching infinity as r approaches zero in figure 12, the deflection is actually approaching zero. Figure 3(a) verifies this observation.

CONCLUSION

This deflection amplification analysis of damped rotors shows that in addition to the major critical speed, a lower-frequency resonance appears if certain design conditions exist. These conditions include symmetrical support stiffness and damping characteristics and equal probability for the distribution of the axial location of the planes of unbalance along with either (1) center of gravity not located at midplane or (2) ratio of polar-to-diametral moment-of-inertia ratio less than 0.7; therefore, the low-frequency resonance should appear for slender rotors but not for disks.

APPENDIX A

SYMBOLS

A_1 $k\left(L_1\pi_1^2 + \pi_{10}\pi_1/2 + 1/2\right)$

A_2 $k\left(L_2\pi_1^2 + \pi_{10}\pi_1/2 + 1/2\right)$

a_1 real part of numerator in eq. (35) for support 1; see eq. (B4)

a_2 real part of numerator in eq. (35) for support 2; see eq. (B6)

B_1 $= k\ell\left(\pi_2\pi_1^2 + \frac{L_1\pi_{10}\pi_1}{2} + \frac{L_1}{2}\right)$

B_2 $= k\ell\left(\pi_2\pi_1^2 + \frac{L_2\pi_{10}\pi_1}{2} + \frac{L_2}{2}\right)$

$b/2$ linear damping coefficient, kg/sec

C $k\ell\pi_1\pi_2\pi_3\pi_4$

c_1 imaginary part of numerator in eq. (35) for support 1, see eq. (B4)

c_2 imaginary part of numerator in eq. (35) for support 2; see eq. (B6)

D denominator of deflection solution; see eq. (22)

e eccentricity causing unbalance

$F(\omega)$ amplitude of harmonic driving force, nt

g real part of denominator in eq. (35)

h imaginary part of denominator in eq. (35)

I_D rotor diametral moment of inertia, kg-m^2

I_p rotor polar moment of inertia, kg-m^2

i $\sqrt{-1}$

k linear spring constant, kg/sec^2

L_1 $= \frac{\ell_1}{\ell}$

L_2 $= \frac{\ell_2}{\ell}$

$\mathcal{L}$ Laplace operator

ℓ distance between bearings, m

M	rotor mass, kg
$\mathcal{M}$	moment, nt-m
N	numerator of deflection solution; see eq. (22)
r	bearing force ratio; see fig. 1
s	Laplace variable, sec^{-1}
t	time, sec
x,y,z	rectangular coordinates defined in fig. 1
Y	$Y(s) = \mathcal{L}[y(t)]$
Z	$Z(s) = \mathcal{L}[z(t)]$
θ	phase angle, deg
μ	deflection amplification factor
π_1	$s/\sqrt{k/M}$
π_2	$I_D/M\ell^2$ = disk effect
π_3	I_p/I_D = rotor polar-to-diametral moment-of-inertia ratio
π_4	$\omega/\sqrt{k/M}$ = rotational-speed parameter
π_{10}	$b/\sqrt{kM}$ = damping parameter
ω	rotor rotational frequency = harmonic driving force frequency, rad/sec

Subscripts:

P	peak
r	condition for $r_y = r_z = r$
y	y direction; see fig. 1
z	z direction; see fig. 1
1,2	supports 1 and 2; see fig. 1

Superscripts:

$\dot{}$ first derivative with respect to time

$\ddot{}$ second derivative with respect to time

APPENDIX B

ANALYSIS DETAILS

General

Expansion of the determinants in equations (24) to (26) yields

$$N_1 = -(r_y + 1)s\left[C^2(A_1 + A_2) + B_2(A_1B_1 + A_2B_2)\right] - (r_z + 1)\omega A_1 C(B_1 - B_2)$$
$$+ A_1[(\ell_2 r_z - \ell_1)\omega C(A_1 + A_2) - (\ell_2 r_y - \ell_1)s(A_1B_1 + A_2B_2)] \qquad (B1)$$

$$N_2 = -(r_y + 1)s\left[C^2(A_1 + A_2) + B_1(A_1B_1 + A_2B_2)\right] + (r_z + 1)\omega A_2 C(B_1 - B_2)$$
$$- A_2[(\ell_2 r_z - \ell_1)\omega C(A_1 + A_2) - (\ell_2 r_y - \ell_1)s(A_1B_1 + A_2B_2)] \qquad (B2)$$

$$D = -C^2(A_1 + A_2)^2 - (A_1B_1 + A_2B_2)^2 \qquad (B3)$$

The values of a and c for Y_1 in equation (35) differ from the values for Y_2

For support 1 (see fig. 1),

$$a_1 = (r_y + 1)\left\{\pi_4^6\left(\pi_3^2 - 1\right)\pi_2^2 + \pi_4^4\left[-\pi_2^2\left(\pi_3^2 - 1\right) + \frac{\left(L_1^2 + L_2^2\right)\pi_2}{2} + \frac{\pi_2\pi_{10}^2}{4}\right.\right.$$
$$\left. + \frac{L_2\left(L_1^2 + L_2^2\right)\pi_{10}^2}{4} + \frac{L_2\pi_2\pi_{10}^2}{2} + \frac{L_2\pi_2}{2}\right] - \pi_4^2\left[\frac{\pi_2}{4} + \frac{L_2\left(L_1^2 + L_2^2\right)}{4} + \frac{3L_2\pi_{10}^2}{8}\right.$$
$$\left.\left. + \frac{L_2\pi_2}{2}\right] + \frac{L_2}{8}\right\} + (r_z + 1)\pi_2\pi_3\left\{-\pi_4^4\left[L_1 + \frac{\pi_{10}^2}{2}\right]\left(\frac{L_1 - L_2}{2}\right) + \pi_4^2\,\frac{L_1 - L_2}{4}\right\}$$
$$+ (r_y L_2 - L_1)\left\{-L_1\pi_2\pi_4^6 + \pi_4^4\left[\frac{L_1\left(L_1^2 + L_2^2\right)}{2} + \frac{L_1\pi_{10}^2}{4} + L_1\pi_2 + \frac{\left(L_1^2 + L_2^2\right)\pi_{10}^2}{4}\right.\right.$$
$$\left. + \frac{\pi_2\pi_{10}^2}{2} + \frac{\pi_2}{2}\right] - \pi_4^2\left[\frac{L_1}{4} + \frac{\left(L_1^2 + L_2^2\right)}{4} + \frac{3\pi_{10}^2}{8} + \frac{\pi_2}{2}\right] + \frac{1}{8}\left.\right\}$$
$$- (r_z L_2 - L_1)\pi_2\pi_3\left[\pi_4^6 L_1 - \pi_4^4\left(L_1 + \frac{\pi_{10}^2}{2} + \frac{1}{2}\right) + \frac{\pi_4^2}{2}\right] \qquad (B4)$$

$$c_1 = (r_y + 1)\left\{\pi_4^5\left(-\pi_2\pi_3^2 + \frac{L_1^2 + L_2^2}{2} + \pi_2 + \frac{L_2}{2}\right)\pi_2 - \pi_4^3\left[\frac{\pi_2}{2} + \frac{L_2\left(L_1^2 + L_2^2\right)}{2}\right.\right.$$
$$\left.\left. + \frac{L_2\pi_{10}^2}{8} + L_2\pi_2\right] + \pi_4\left(\frac{3L_2}{8}\right)\right\}\pi_{10} + (r_z + 1)\pi_2\pi_3\left(-\pi_4^5 L_1 + \pi_4^3\right)\left(\frac{L_1 - L_2}{2}\right)\pi_{10}$$
$$+ (r_y L_2 - L_1)\left\{\pi_4^5\left[\frac{L_1\left(L_1^2 + L_2^2\right)}{2} + L_1\pi_2 + \frac{\pi_2}{2}\right] - \pi_4^3\left(\frac{L_1}{2} + \frac{L_1^2 + L_2^2}{2} + \frac{\pi_{10}^2}{8} + \pi_2\right)\right.$$
$$\left. + \pi_4\left(\frac{3}{8}\right)\right\}\pi_{10} + (r_z L_2 - L_1)\pi_2\pi_3\pi_{10}\left[\pi_4^5\left(L_1 + \frac{1}{2}\right) - \pi_4^3\right] \qquad \text{(B5)}$$

For support 2,

$$a_2 = -(r_y + 1)\left\{\pi_4^6\left(\pi_3^2 - 1\right)\pi_2^2 + \pi_4^4\left[-\pi_2^2\left(\pi_3^2 - 1\right) + \frac{\left(L_1^2 + L_2^2\right)\pi_2}{2} + \frac{\pi_2\pi_{10}^2}{4}\right.\right.$$
$$+ \frac{L_1\left(L_1^2 + L_2^2\right)\pi_{10}^2}{4} + \frac{L_1\pi_2\pi_{10}^2}{2} + \frac{L_1\pi_2}{2}\left] - \pi_4^2\right[\frac{\pi_2}{4} + \frac{L_1\left(L_1^2 + L_2^2\right)}{4} + \frac{3L_1\pi_{10}^2}{8}$$
$$\left.\left. + \frac{L_1\pi_2}{2}\right] + \frac{L_1}{8}\right\} + (r_z + 1)\pi_2\pi_3\left\{-\pi_4^4\left[L_2 + \frac{\pi_{10}^2}{2}\right]\left(\frac{L_1 - L_2}{2}\right) + \pi_4^2\left(\frac{L_1 - L_2}{4}\right)\right\}$$
$$+ (r_y L_2 - L_1)\left\{-\pi_4^6 L_2\pi_2 + \pi_4^4\left[\frac{L_2\left(L_1^2 + L_2^2\right)}{2} + \frac{L_2\pi_{10}^2}{4} + L_2\pi_2 + \frac{\left(L_1^2 + L_2^2\right)\pi_{10}^2}{4}\right.\right.$$
$$\left.\left. + \frac{\pi_2\pi_{10}^2}{2} + \frac{\pi_2}{2}\right] - \pi_4^2\left[\frac{L_2}{4} + \frac{\left(L_1^2 + L_2^2\right)}{4} + \frac{3\pi_{10}^2}{8} + \frac{\pi_2}{2}\right] + \frac{1}{8}\right\}$$
$$- (r_z L_2 - L_1)\pi_2\pi_3\left[\pi_4^6 L_2 - \pi_4^4\left(L_2 + \frac{\pi_{10}^2}{2} + \frac{1}{2}\right) + \frac{\pi_4^2}{2}\right] \qquad \text{(B6)}$$

$$c_2 = -(r_y + 1)\left\{\pi_4^5\left(-\pi_2\pi_3^2 + \frac{L_1^2 + L_2^2}{2} + \pi_2 + \frac{L_1}{2}\right)\pi_2 - \pi_4^3\left[\frac{\pi_2}{2} + \frac{L_1\left(L_1^2 + L_2^2\right)}{2}\right.\right.$$

$$\left.\left. + \frac{L_1\pi_{10}^2}{8} + L_1\pi_2\right] + \pi_4\left(\frac{3L_1}{8}\right)\right\}\pi_{10} + (r_z + 1)\pi_2\pi_3\left(-\pi_4^5 L_2 + \pi_4^3\right)\frac{(L_1 - L_2)\pi_{10}}{2}$$

$$+ (r_y L_2 - L_1)\left\{\pi_4^5\left[\frac{L_2\left(L_1^2 + L_2^2\right)}{2} + L_2\pi_2 + \frac{\pi_2}{2}\right] - \pi_4^3\left[\frac{L_2}{2} + \frac{\left(L_1^2 + L_2^2\right)}{2}\right.\right.$$

$$\left.\left. + \frac{\pi_{10}^2}{8} + \pi_2\right] + \pi_4\left(\frac{3}{8}\right)\right\}\pi_{10} + (r_z L_2 - L_1)\pi_2\pi_3\pi_{10}\left[\pi_4^5\left(L_2 + \frac{1}{2}\right) - \pi_4^3\right] \quad \text{(B7)}$$

For each support, the denominator D has components

$$g = \pi_4^8\left(\pi_3^2 - 1\right)\pi_2^2 - \pi_4^6\left[-\pi_2^2\pi_3^2\left(2 + \pi_{10}^2\right) + \pi_2^2\pi_{10}^2 + \frac{\left(L_1^2 + L_2^2\right)^2\pi_{10}^2}{4}\right.$$

$$\left. + \left(L_1^2 + L_2^2\right)\pi_2\left(1 + \pi_{10}^2\right) + \frac{\pi_2\pi_{10}^2}{2} + 2\pi_2^2\right] + \pi_4^4\left[\frac{\left(L_1^2 + L_2^2\right)^2}{4} + \frac{\pi_{10}^4}{16}\right.$$

$$\left. - \pi_2^2\left(\pi_3^2 - 1\right) + \frac{\pi_2}{2} + \left(L_1^2 + L_2^2\right)\left(\frac{3\pi_{10}^2}{4} + \pi_2\right) + \frac{3\pi_2\pi_{10}^2}{2}\right]$$

$$- \pi_4^2\left[\frac{L_1^2 + L_2^2}{4} + \frac{3\pi_{10}^2}{8} + \frac{\pi_2}{2}\right] + \frac{1}{16} \quad \text{(B8)}$$

$$h = \pi_{10}\left\{-\pi_4^7\left[-\left(\pi_3^2 - 1\right)2\pi_2 + \left(L_1^2 + L_2^2\right)\right]\pi_2 + \pi_4^5\left[\pi_2 + \frac{\left(L_1^2 + L_2^2\right)^2}{2}\right.\right.$$

$$\left. + \left(L_1^2 + L_2^2\right)\left(\frac{\pi_{10}^2}{4} + 2\pi_2\right) + \frac{\pi_2\pi_{10}^2}{2} - 2\pi_2^2\left(\pi_3^2 - 1\right)\right]$$

$$\left. + \frac{\pi_4^3}{2}\left[\frac{3\left(L_1^2 + L_2^2\right)}{2} + \frac{\pi_{10}^2}{2} + 3\pi_2\right] + \frac{\pi_4}{4}\right\} \quad \text{(B9)}$$

Restriction: $r_y = r_z = r$

All the calculated results presented in this report were obtained for the condition

$$r_y = r_z = r \tag{B10}$$

Therefore, the values of a and c as modified by this condition are presented below.

Support 1. -

$$a_{1r} = (r + 1)\left\{\pi_4^6\left(\pi_3^2 - 1\right)\pi_2^2 + \pi_4^4\left[-\pi_2^2\left(\pi_3^2 - 1\right) + \frac{\left(L_1^2 + L_2^2\right)\pi_2}{2} + \frac{\pi_2\pi_{10}^2}{4}\right.\right.$$

$$\left. + \frac{L_2\left(L_1^2 + L_2^2\right)\pi_{10}^2}{4} + \frac{L_2\pi_2}{2}\left(\pi_{10}^2 + 1\right) - \pi_2\pi_3\left(L_1 + \frac{\pi_{10}^2}{2}\right)\left(\frac{L_1 - L_2}{2}\right)\right] - \pi_4^2\left[\frac{\pi_2}{4}\right.$$

$$\left.\left. + \frac{L_2\left(L_1^2 + L_2^2\right)}{4} + \frac{3L_2\pi_{10}^2}{8} + \frac{L_2\pi_2}{2} - \pi_2\pi_3\left(\frac{L_1 - L_2}{4}\right)\right] + \frac{L_2}{8}\right\}$$

$$+ (rL_2 - L_1)\left\{-\pi_4^6 L_1\pi_2(\pi_3 + 1) + \pi_4^4\left[\left(\frac{L_1^2 + L_2^2}{2}\right)\left(L_1 + \frac{\pi_{10}^2}{2}\right)\right.\right.$$

$$\left. + L_1\left(\frac{\pi_{10}^2}{4} + \pi_2\right) + \frac{\pi_2\pi_{10}^2}{2}(\pi_3 + 1) + \pi_2\pi_3\left(L_1 + \frac{1}{2}\right) + \frac{\pi_2}{2}\right]$$

$$\left. - \pi_4^2\left[\frac{L_1}{4} + \frac{L_1^2 + L_2^2}{4} + \frac{3\pi_{10}^2}{8} + \frac{\pi_2}{2}(\pi_3 + 1) + \frac{1}{8}\right]\right\} \tag{B11}$$

$$c_{1r} = (r+1)\left\{\pi_4^5\left[-\pi_2\left(\pi_3^2 - 1\right) + \frac{L_1^2 + L_2^2}{2} + \frac{L_2}{2} - L_1\pi_3\left(\frac{L_1 - L_2}{2}\right)\right]\pi_2\right.$$

$$- \pi_4^3\left[\frac{\pi_2}{2} + \frac{L_2\left(L_1^2 + L_2^2\right)}{2} + \frac{L_2\pi_{10}^2}{8} + L_2\pi_2 - \pi_2\pi_3\pi_{10}\left(\frac{L_1 - L_2}{2}\right)\right] + \pi_4\left(\frac{3L_2}{8}\right)\Bigg\}\pi_{10}$$

$$+ (rL_2 - L_1)\left\{\pi_4^5\left[\frac{L_1\left(L_1^2 + L_2^2\right)}{2} + L_1\pi_2 + \frac{\pi_2}{2} + \pi_2\pi_3\left(L_1 + \frac{1}{2}\right)\right]\right.$$

$$\left. - \pi_4^3\left[\frac{L_1}{2} + \frac{L_1^2 + L_2^2}{2} + \frac{\pi_{10}^2}{8} + \pi_2(\pi_3 + 1)\right] + \pi_4\left(\frac{3}{8}\right)\right\}\pi_{10} \qquad \text{(B12)}$$

Support 2. -

$$a_{2r} = -(r+1)\left\{\pi_4^6\left(\pi_3^2 - 1\right)\pi_2^2 + \pi_4^4\left[-\pi_2^2\left(\pi_3^2 - 1\right) + \frac{\left(L_1^2 + L_2^2\right)\pi_2}{2} + \frac{\pi_2\pi_{10}^2}{4}\right.\right.$$

$$\left. + \frac{L_1\left(L_1^2 + L_2^2\right)\pi_{10}^2}{4} + \frac{L_1\pi_2}{2}\left(\pi_{10}^2 + 1\right) + \pi_2\pi_3\left(L_2 + \frac{\pi_{10}^2}{2}\right)\left(\frac{L_1 - L_2}{2}\right)\right]$$

$$- \pi_4^2\left[\frac{\pi_2}{4} + \frac{L_1\left(L_1^2 + L_2^2\right)}{4} + \frac{3L_1\pi_{10}^2}{8} + \frac{L_1\pi_2}{2} - \pi_2\pi_3\left(\frac{L_1 - L_2}{4}\right)\right] + \frac{L_1}{8}\Bigg\}$$

$$+ (rL_2 - L_1)\left\{-\pi_4^6 L_2\pi_2(\pi_3 + 1) + \pi_4^4\left[\frac{L_1^2 + L_2^2}{2}\left(L_2 + \frac{\pi_{10}^2}{2}\right) + L_2\left(\frac{\pi_{10}^2}{4} + \pi_2\right)\right.\right.$$

$$\left. + \frac{\pi_2\pi_{10}^2}{2}(\pi_3 + 1) + \pi_2\pi_3\left(L_2 + \frac{1}{2}\right) + \frac{\pi_2}{2}\right]$$

$$\left. - \pi_4^2\left[\frac{L_2}{4} + \frac{L_1^2 + L_2^2}{4} + \frac{3\pi_{10}^2}{8} + \frac{\pi_2}{2}(\pi_3 + 1)\right] + \frac{1}{8}\right. \qquad \text{(B13)}$$

$$c_{2r} = -(r + 1)\left\{\pi_4^5\left[-\pi_2\left(\pi_3^2 - 1\right) + \frac{L_1^2 + L_2^2}{2} + \frac{L_1}{2} - L_2\pi_3\left(\frac{L_1 - L_2}{2}\right)\right]\pi_2\right.$$

$$- \pi_4^3\left[\frac{\pi_2}{2} + \frac{L_1\left(L_1^2 + L_2^2\right)}{2} + \frac{L_1\pi_{10}^2}{8} + L_1\pi_2 - \pi_2\pi_3\left(\frac{L_1 - L_2}{2}\right)\right] + \pi_4\left(\frac{3L_1}{8}\right)\Bigg\}\pi_{10}$$

$$+ (rL_2 - L_1)\left\{\pi_4^5\left[\frac{L_2\left(L_1^2 + L_2^2\right)}{2} + L_2\pi_2 + \frac{\pi_2}{2} + \pi_2\pi_3\left(L_2 + \frac{1}{2}\right)\right]\right.$$

$$\left. - \pi_4^3\left[\frac{L_2}{2} + \frac{L_1^2 + L_2^2}{2} + \frac{\pi_{10}^2}{8} + \pi_2\left(\pi_3 + 1\right)\right] + \pi_4\left(\frac{3}{8}\right)\right\}\pi_{10} \qquad \text{(B14)}$$

Normalizing factors. - Displacement magnitudes are normalized by division by the magnitude at zero rotational speed. This condition requires that

$$\pi_4 = 0 \qquad \text{(B15)}$$

Therefore, for support 1

$$\left|\frac{N_1}{D}\right|_{\pi_4=0} = 2[L_2(2r + 1) - L_1] \qquad \text{(B16)}$$

and for support 2

$$\left|\frac{N_2}{D}\right|_{\pi_4=0} = 2[r(L_2 - L_1) - 2L_1] \qquad \text{(B17)}$$

Setting each of the last two equations equal to zero gives the value of r for zero deflection at each support. From equation (B16)

$$r_{N_1=0} = \frac{1}{2}\left(\frac{L_1}{L_2} - 1\right) \qquad \text{(B18)}$$

From equation (B17)

$$r_{N_2=0} = \frac{2}{\frac{L_2}{L_1} - 1} \tag{B19}$$

Finally, equating these two equations to each other yields

$$\frac{L_1}{L_2} + \frac{L_2}{L_1} = -2 \tag{B20}$$

Physically, this set of conditions is impossible because although L_2 can be less than 1,

$$|L_1| \geq |L_2|$$

Therefore, there is no set of conditions for which

$$\left|\frac{N_1}{D}\right|_{\pi_4=0} = \left|\frac{N_2}{D}\right|_{\pi_4=0}$$

TABLE I. - PARAMETER SELECTIONS

Case	π_2 $I_D/M\ell^2$	π_3 I_p/I_D	π_{10} $b/\sqrt{kM}$	L_1 ℓ_1/ℓ	L_2 ℓ_2/ℓ	$r_y = r_z = r$ F_2/F_1
	Rotor shape		Damping	C.G.	Location	Bearing force ratio
1	1	2	0,0.01,0.1,0.2, 0.5,0.8,1,$\sqrt{2}$,2,3	0.5	0.5	1
2	1	2	case 1 variation	0.5	0.5	0
3	1	2	case 1 variation	0.5	0.5	2
4	1	2	0.1	0.5,0.75 1,1.25	$1-L_1$	2
5	1	2	case 1 variation	1	0	2
6	1	0,0.1,0.5, 1,1.5,2	0.1	0.5	0.5	2
7	0,0.05,0.1,0.2, 0.5,1,10	2	0.1	0.5	0.5	2

REFERENCES

1. Cavicchi, Richard H.: Critical-Speed Analysis of Flexibly-Mounted Rigid Rotors. NASA TN D-4607, 1968.

2. Yamamoto, Toshio: On the Critical Speeds of a Shaft. Memoirs Faculty Eng., Nagoya Univ., vol. 6, no. 2, Nov. 1954, pp. 106-174.

3. Gunter, Edgar J., Jr.: Dynamic Stability of Rotor-Bearing Systems. NASA SP-113, 1966.

4. Cavicchi, Richard H.: Critical-Speed Analysis of Rigid Rotors on Flexible Foundations. NASA TN D-4858, 1969.

5. Cavicchi, Richard H.: Comparison of Flexible- and Firm-Foundation Rotor Critical-Speed Analyses. Paper 69-VIBR-49, ASME, Mar. 1969.

6. Gunter, Edgar J., Jr.; and DeChoudhury, P.: Rigid Rotor Dynamics. NASA CR-1391, 1969.

7. Frost, A.; Lund, J. W.; and Curwen, P. W.: High-Performance Turbo-alternator and Associated Hardware. Volume 2 - Design of Gas Bearings. NASA CR-1291, 1969.

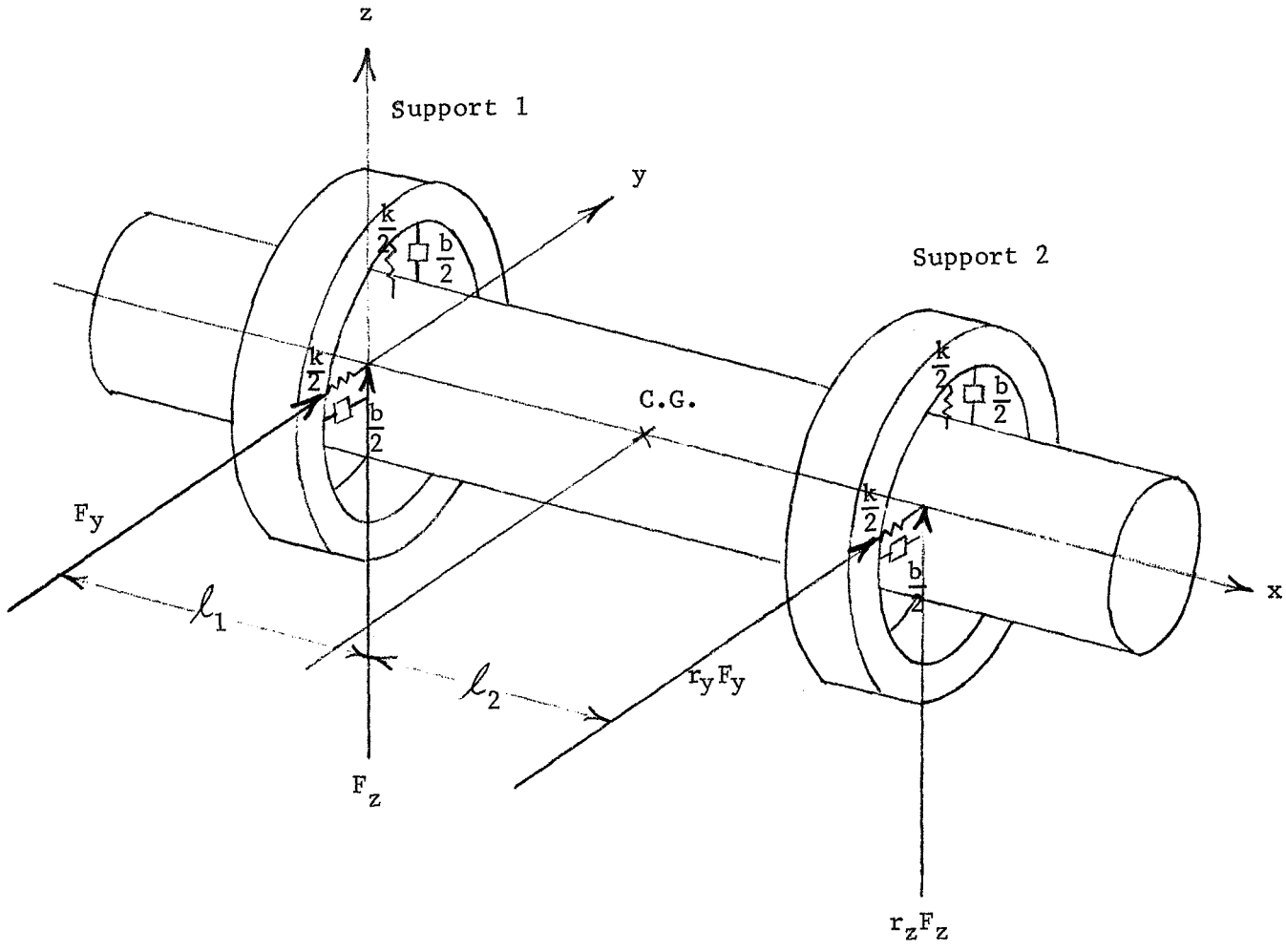

FIGURE 1. SKETCH OF SUPPORT SYSTEM SHOWING FORCE COMPONENTS

Figure 2.- Effect of damping parameter for $r_\gamma = r_z = 1$, case 1.

(a) Support 1 and 2 deflection amplification.

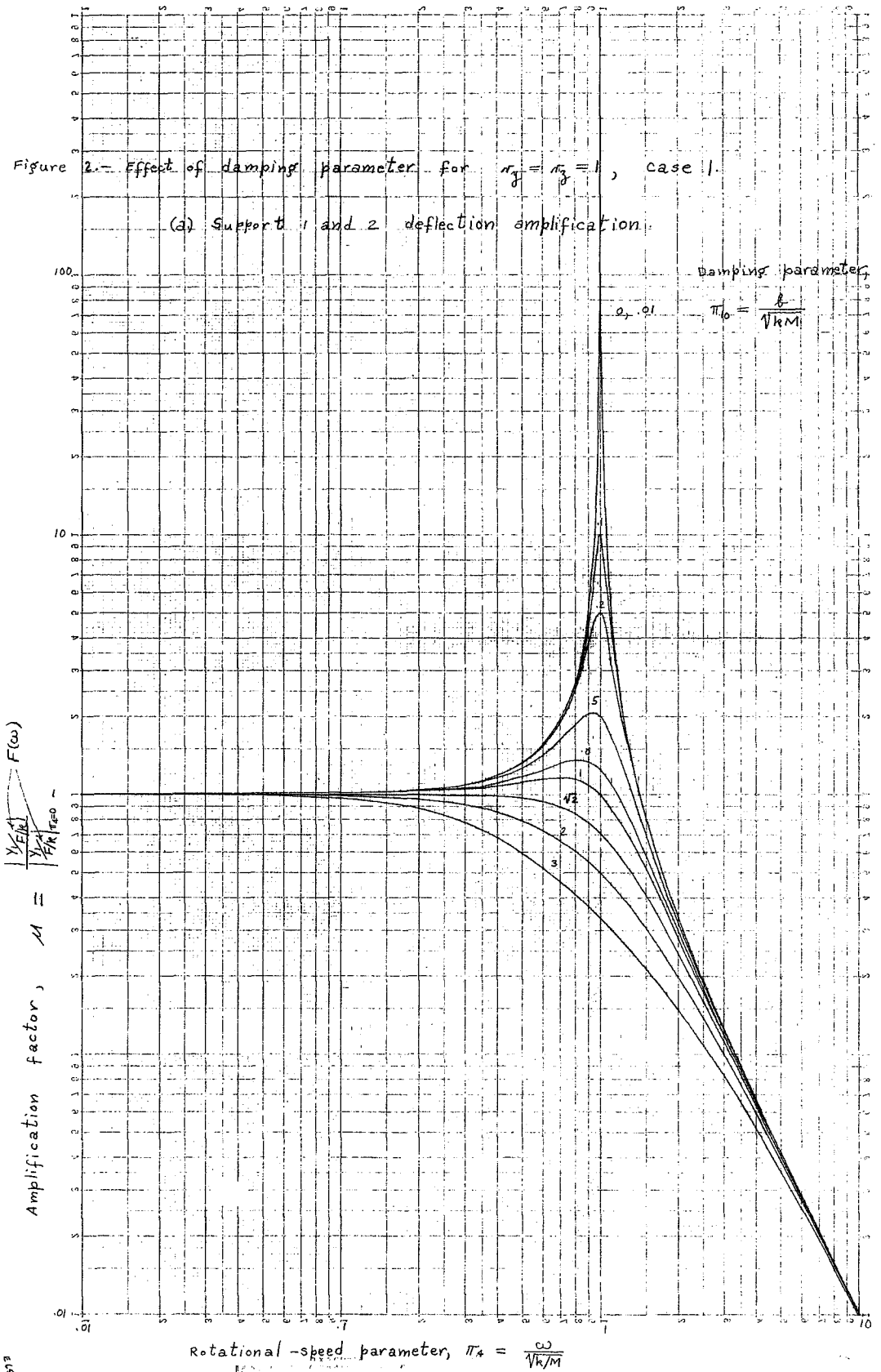

1 Dec. 69

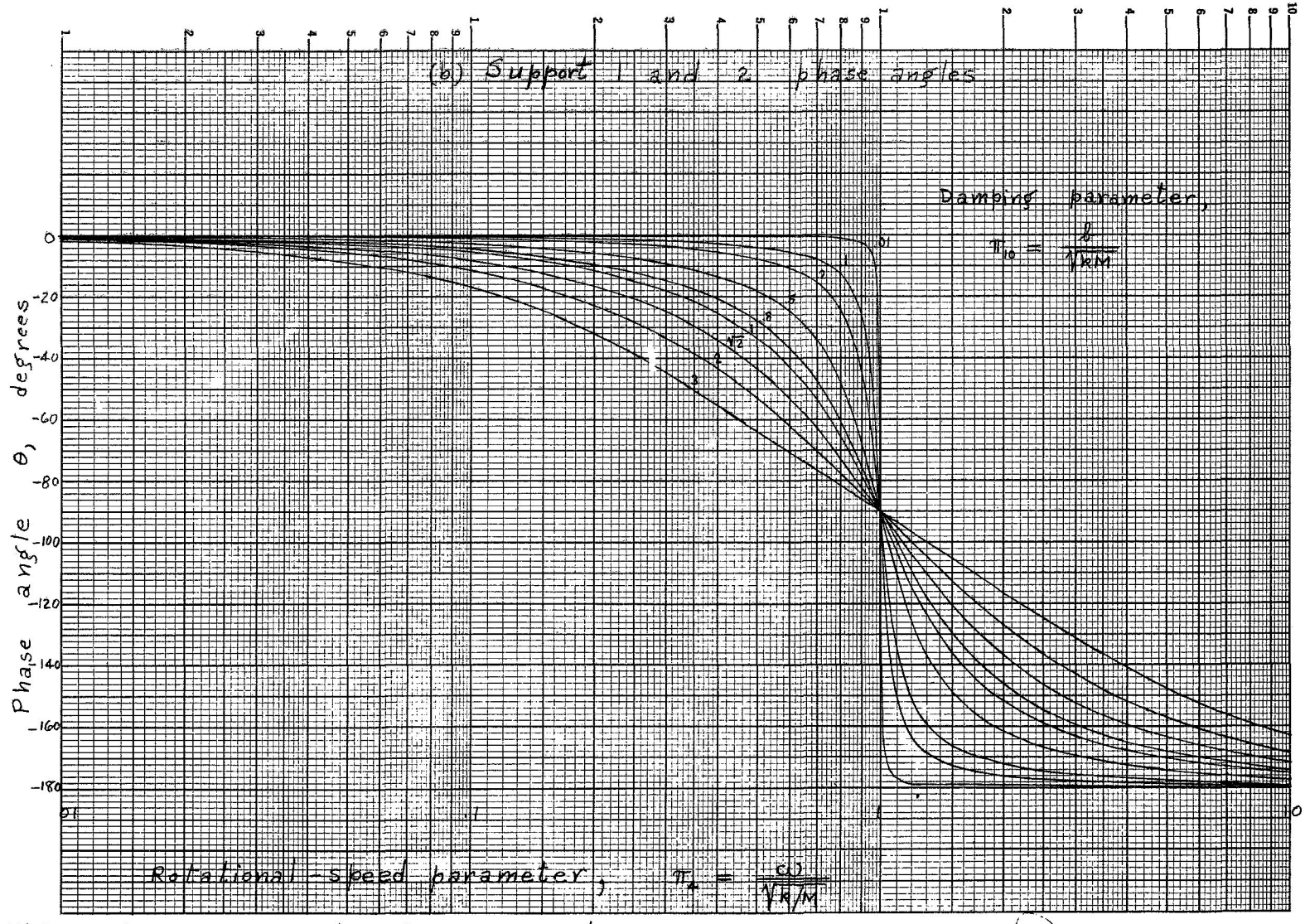

Fig. 2. Concl.- Effect of damping parameter for $r_y = r_z = 1$, case (2.)

2 Dec. 69

Figure 3.- Effect of damping parameter for $r_y = r_z = 0$, case 2.
(a. Support 1 deflection-speed parameter

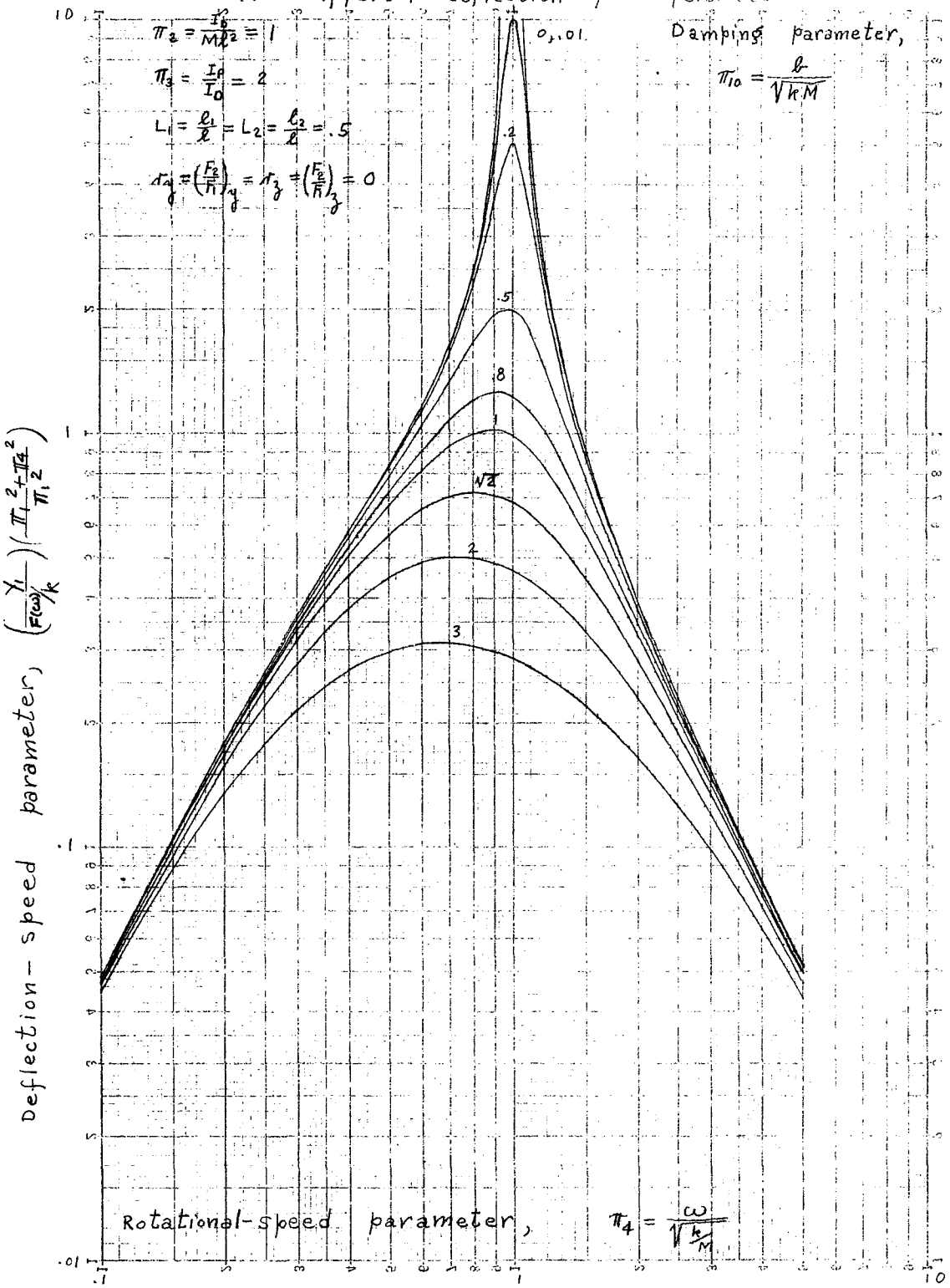

25 MAR. 69

E-6504

Figure 3 [illegible] of damping parameter for $\pi_4 = \pi_3 = 0$, case 2.
(b) support 2 deflection amplification.
Continued.

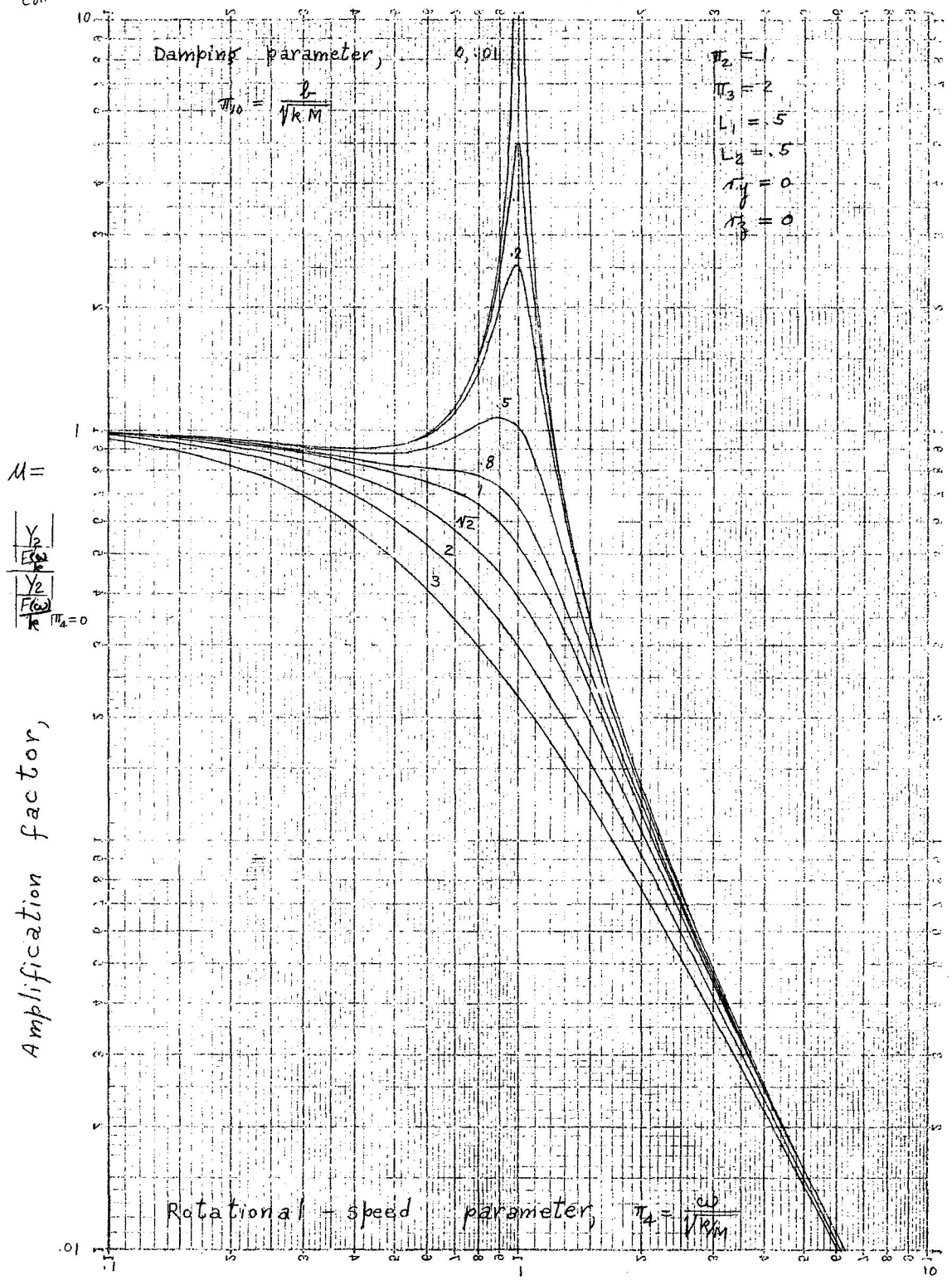

KEUFFEL & ESSER CO. MADE IN U.S.A.
FOLDRITE 328-115

26 MAY 69

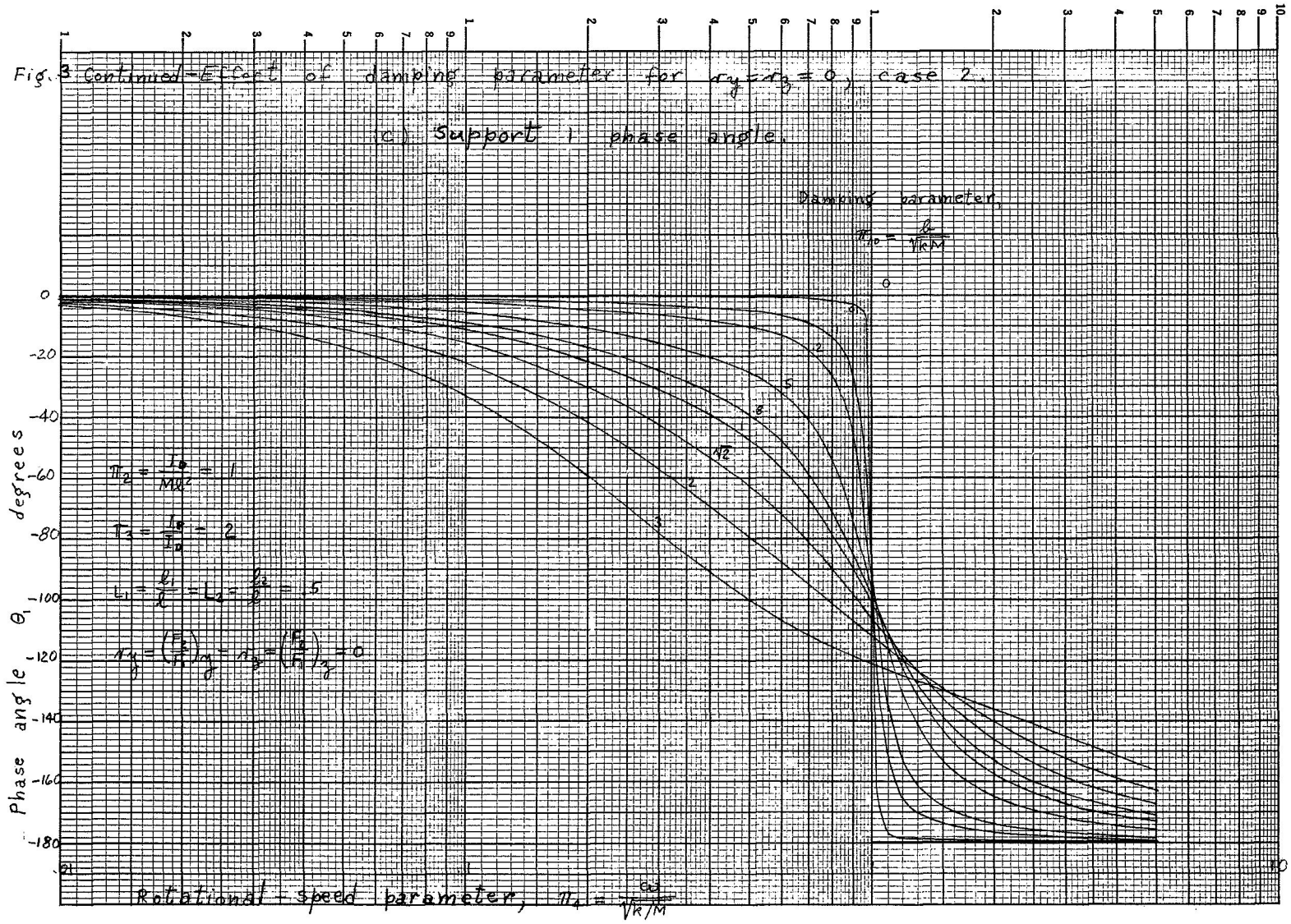
Fig. 3 Continued - Effect of damping parameter for $r_y = r_z = 0$, case 2.
(c) Support 1 phase angle.
Damping parameter, $\pi_{1,0} = \frac{\beta}{\sqrt{kM}}$
0
.5
2
5
8
$\sqrt{2}$
2
3
Phase angle θ_1, degrees
0
-20
-40
-60
-80
-100
-120
-140
-160
-180
$\pi_2 = \frac{I_0}{MR^2} = 1$
$\pi_3 = \frac{I_0}{I_a} = 2$
$L_1 = \frac{\ell_1}{\ell} = L_2 = \frac{\ell_2}{\ell} = .5$
$\pi_4 = \left(\frac{F_2}{F_1}\right)_{xy} = \pi_5 = \left(\frac{F_2}{F_1}\right)_{xz} = 0$
.01
1
10
Rotational - speed parameter, $\pi_4 = \frac{\omega_d}{\sqrt{k/M}}$

25 MAR. 69

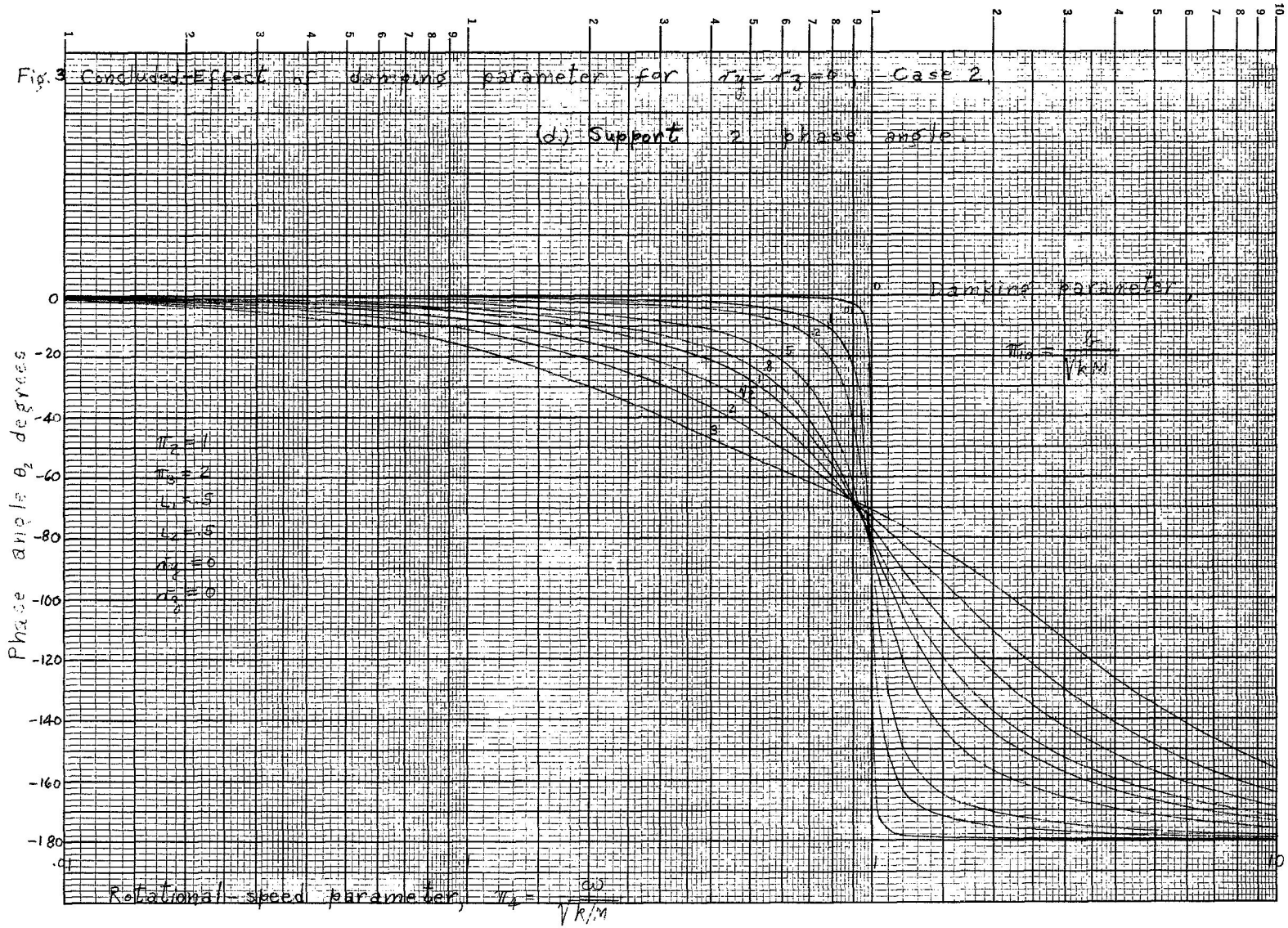

26 MAY 69

Figure 4 - Effect of damping parameter for $\pi_2 = \pi_3 = 2$, case 3.

(a) Support 1 deflection amplification.

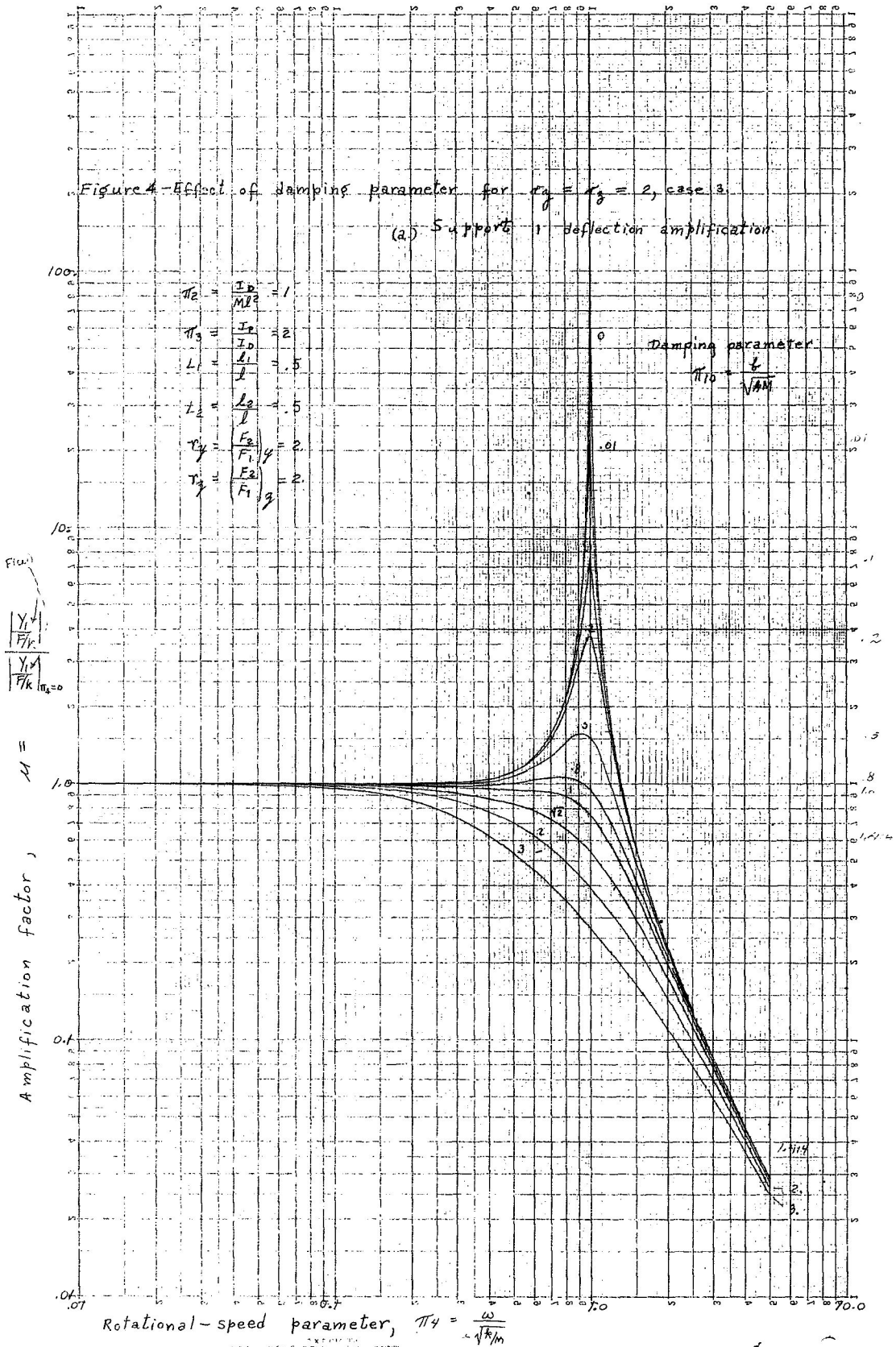

RC-dh
3-13-69

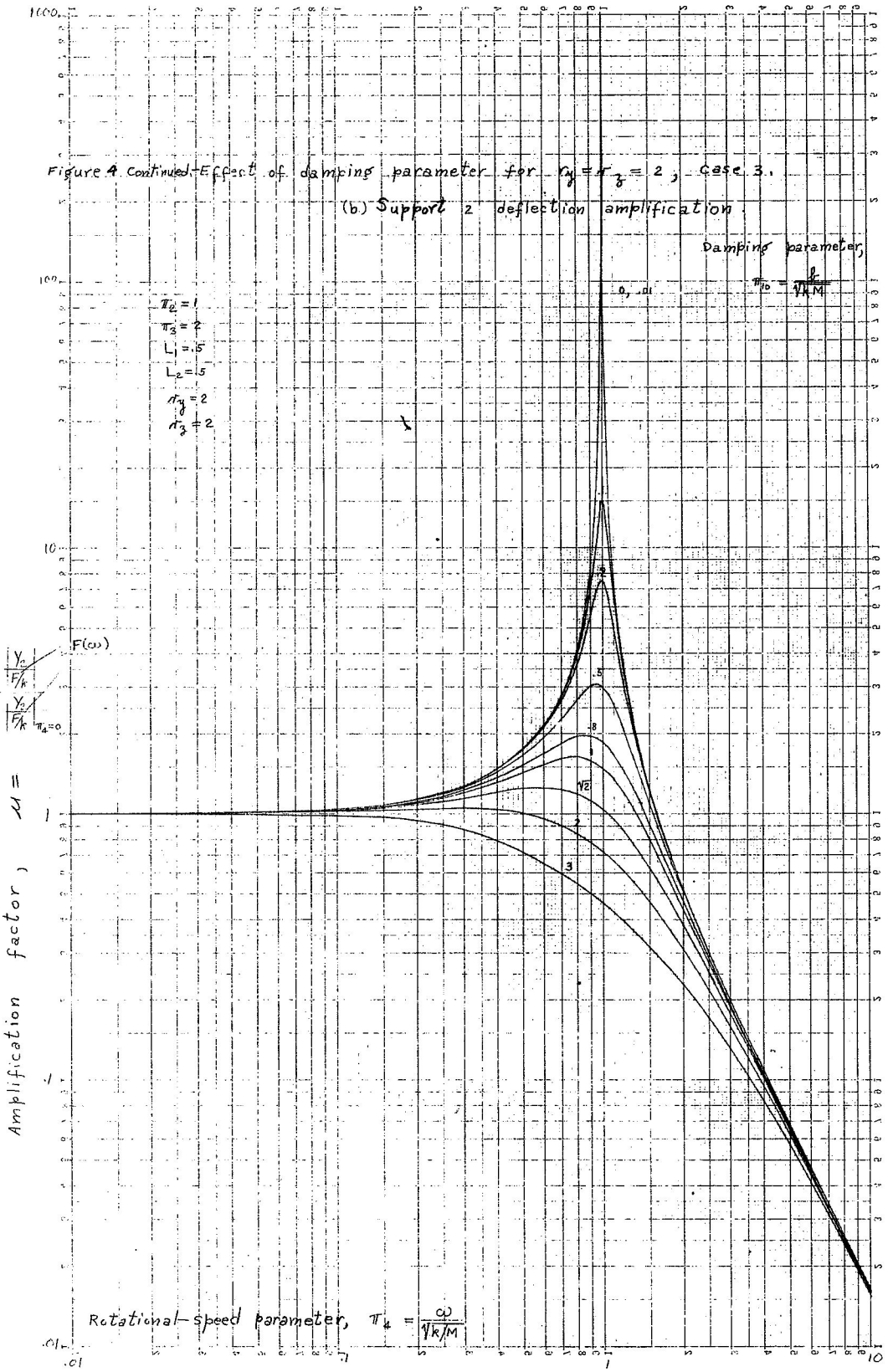
Figure 4 Continued. Effect of damping parameter for $r_y = r_z = 2$, case 3.
(b) Support 2 deflection amplification.
Damping parameter, $\pi_{10} = \frac{f}{\sqrt{kM}}$
0, .01
.1
.5
.8
√2
2
3
$\pi_2 = 1$
$\pi_3 = 2$
$L_1 = .5$
$L_2 = .5$
$r_y = 2$
$r_z = 2$
$\frac{Y_2}{F/k}$ F(ω)
$\frac{Y_2}{F/k}$ $\pi_4 = 0$
Amplification factor, μ =
Rotational-speed parameter, $\pi_4 = \frac{\omega}{\sqrt{k/M}}$
1000
100
10
1
.1
.01
.01
.1
1
10

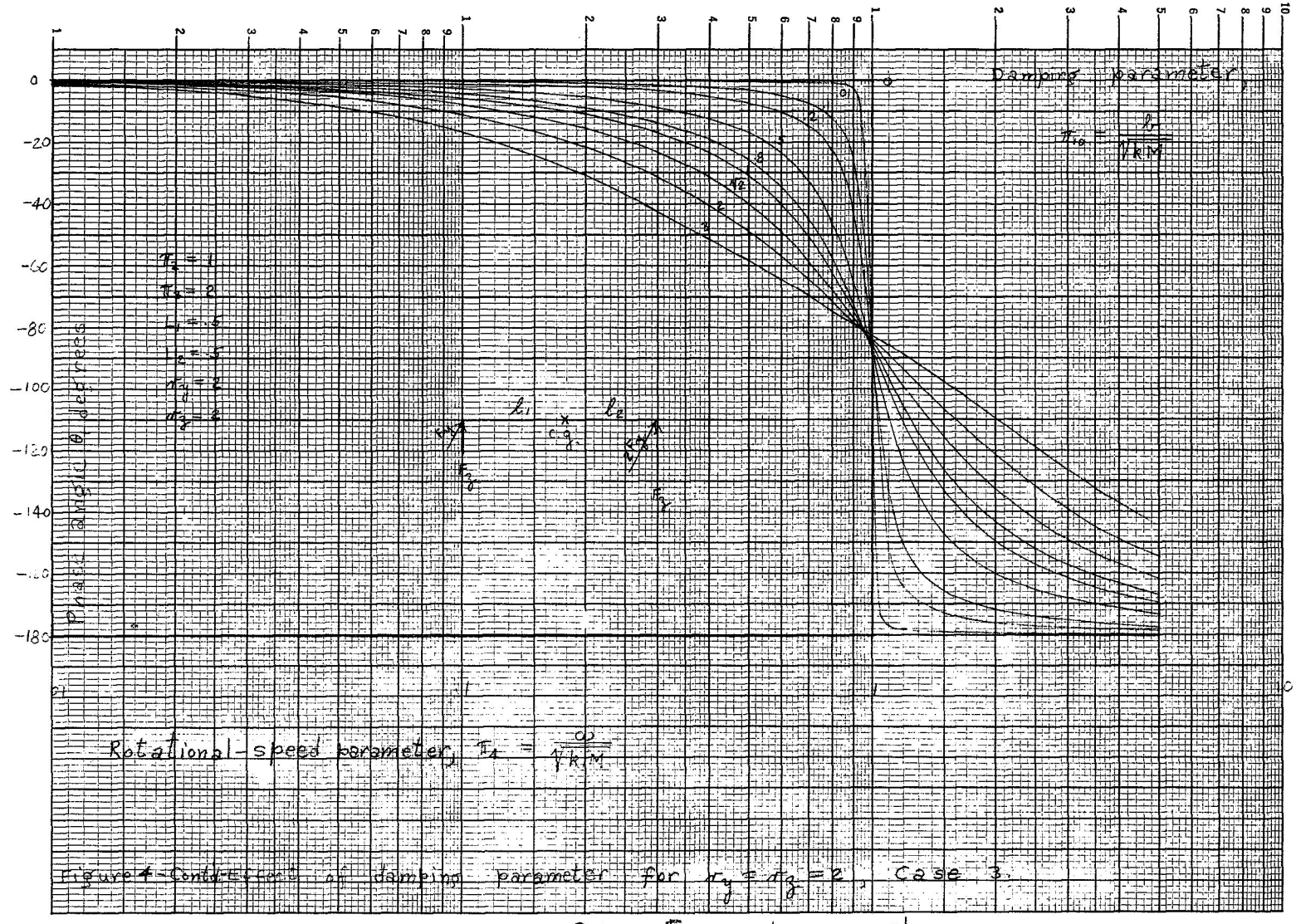

Figure 4.- Continued. Effect of damping parameter for $r_{y_1} = r_{y_2} = 2$, case 3.

(c) Support 1 phase angle.

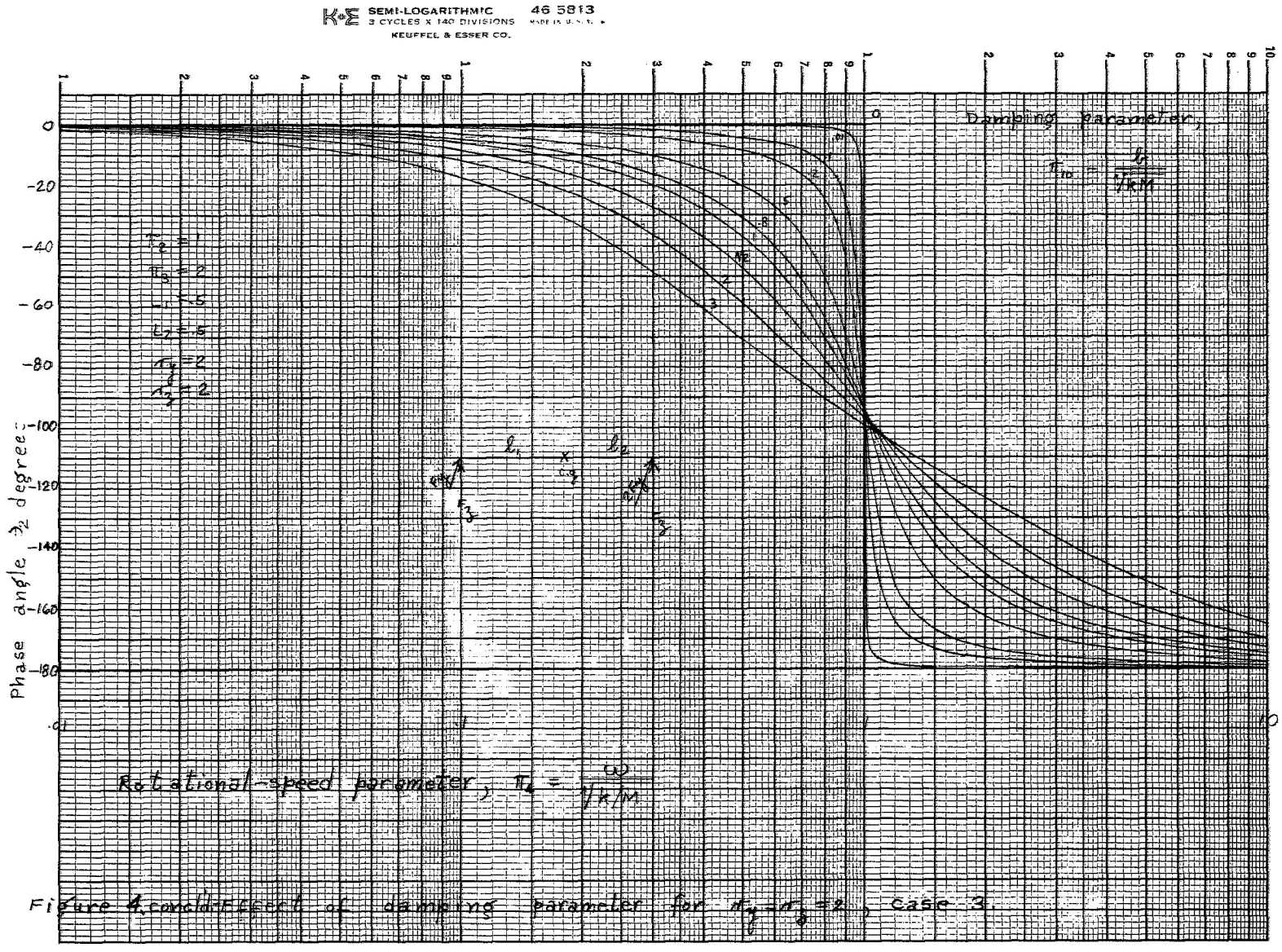

Figure 4.- Concluded. Effect of damping parameter for $\pi_9 = \pi_{10} = 2$, case 3.

(d) Support 2 phase angle.

23 MAY 69

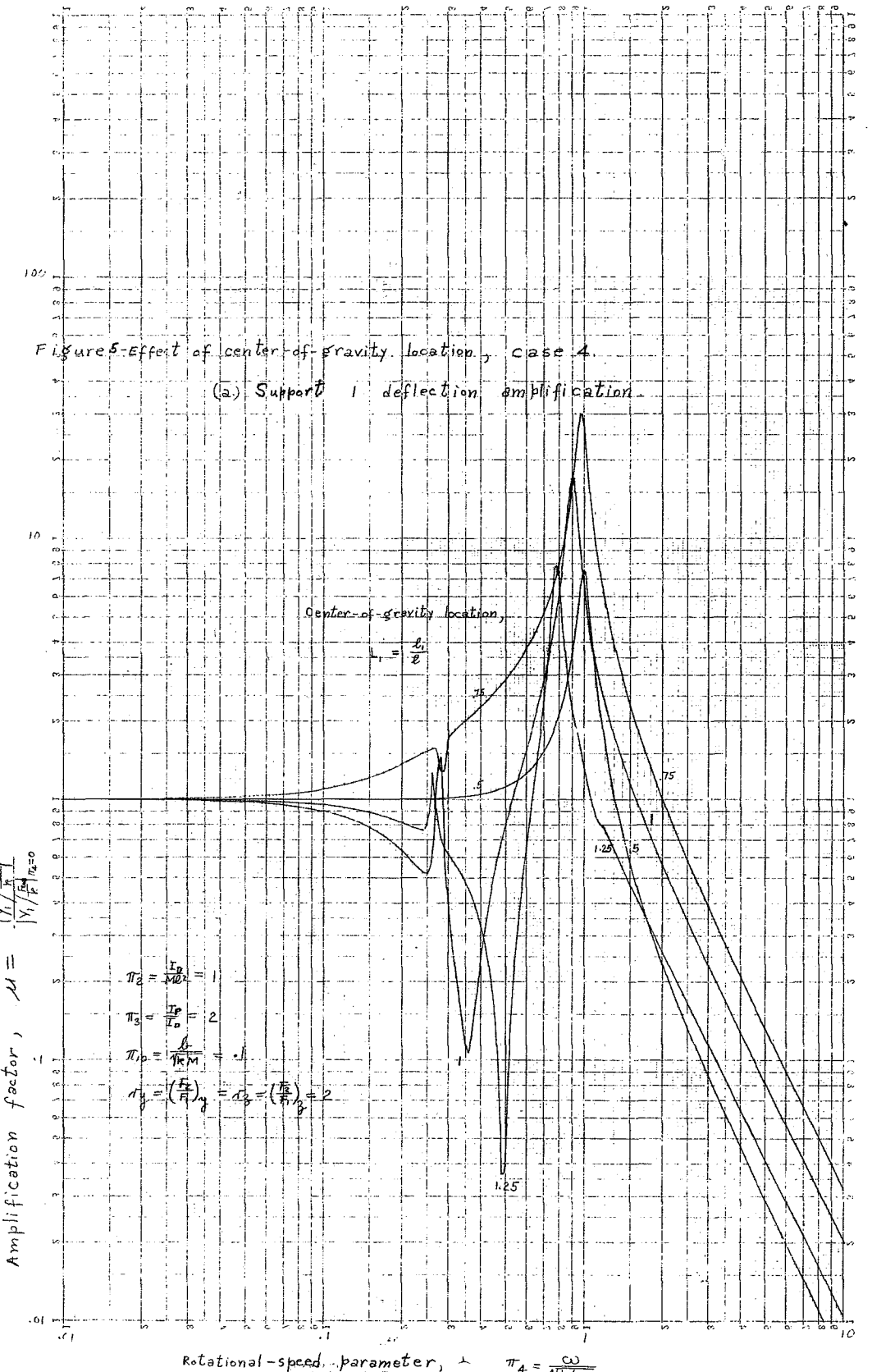
Figure 5-Effect of center-of-gravity location, case 4.
(a) Support 1 deflection amplification.
Amplification factor, $\mu = \left|\frac{Y_1/\frac{F\omega^2}{k}}{Y_1/\frac{F}{k}}\right|_{\pi_4=0}$
Center-of-gravity location, $L_1 = \frac{\ell_1}{\ell}$
.75
.5
.75
1
1.25
.5
1
1.25
$\pi_2 = \frac{I_p}{M\ell^2} = 1$
$\pi_3 = \frac{I_p}{I_o} = 2$
$\pi_{10} = \frac{\ell}{\sqrt{k/M}} = .1$
$r_y = \left(\frac{r_2}{r_1}\right)_y = r_3 = \left(\frac{r_2}{r_1}\right)_\theta = 2$
Rotational-speed parameter, $\pi_4 = \frac{\omega}{\sqrt{k/M}}$

9 sep. 69

E-6504

Figure 5. Cont'd- Effect of center-of-gravity location, case 4.
(b) Support 2 deflection amplification.

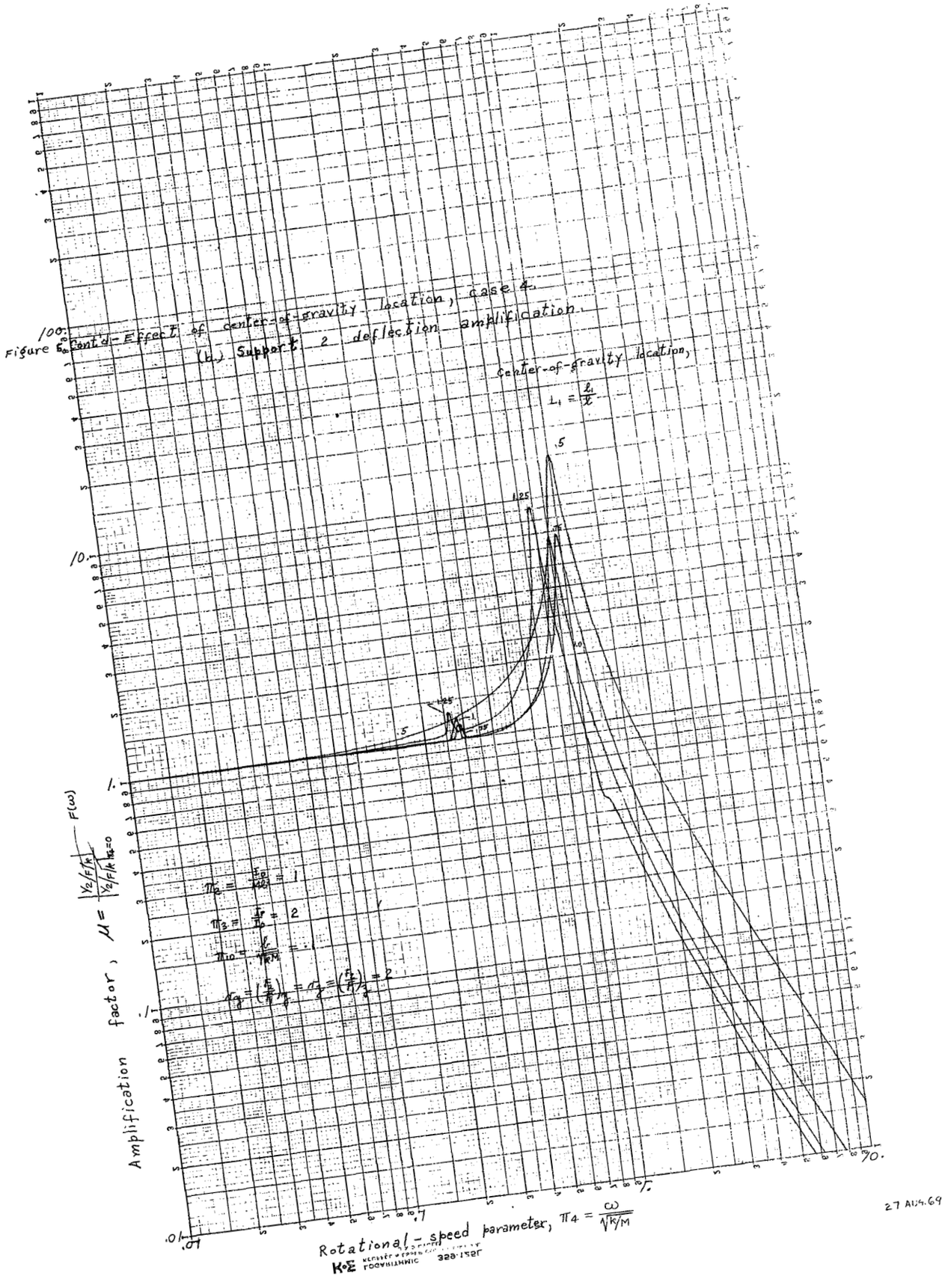

27 AUG 69

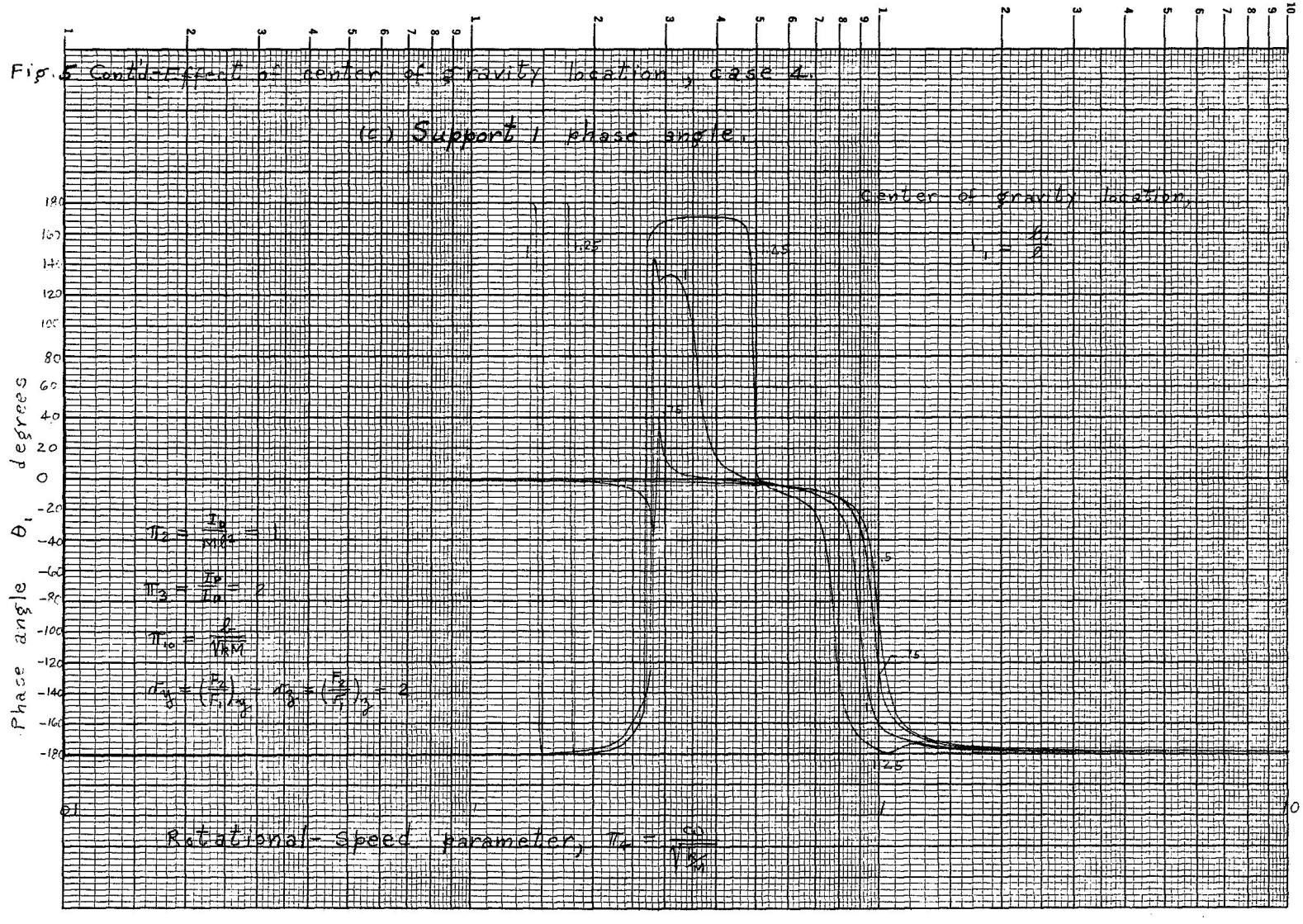
K&E SEMI-LOGARITHMIC 46 5813
3 CYCLES X 140 DIVISIONS MADE IN U.S.A.
KEUFFEL & ESSER CO.
Fig. 5 Contd.-Effect of center of gravity location, case 4.
(c) Support 1 phase angle.
Center of gravity location, $l_1 = \frac{l_1}{l}$
Phase angle θ_1 degrees
180
160
140
120
100
80
60
40
20
0
-20
-40
-60
-80
-100
-120
-140
-160
-180
.125
.25
.5
.75
1
$\pi_2 = \frac{I_p}{Mk^2} = 1$
$\pi_3 = \frac{\pi_9}{\pi_8} = 2$
$\pi_{10} = \frac{\Omega}{\sqrt{\frac{k}{M}}}$
$\pi_{9_2} = \left(\frac{\pi_2}{\pi_1}\right)_{\pi_3} \quad \pi_{8_2} = \left(\frac{\pi_2}{\pi_1}\right)_{\pi_3} = 2$
Rotational-Speed parameter, $\pi_4 = \frac{\Omega}{\sqrt{\frac{k}{M}}}$
10

10 Sept. 69

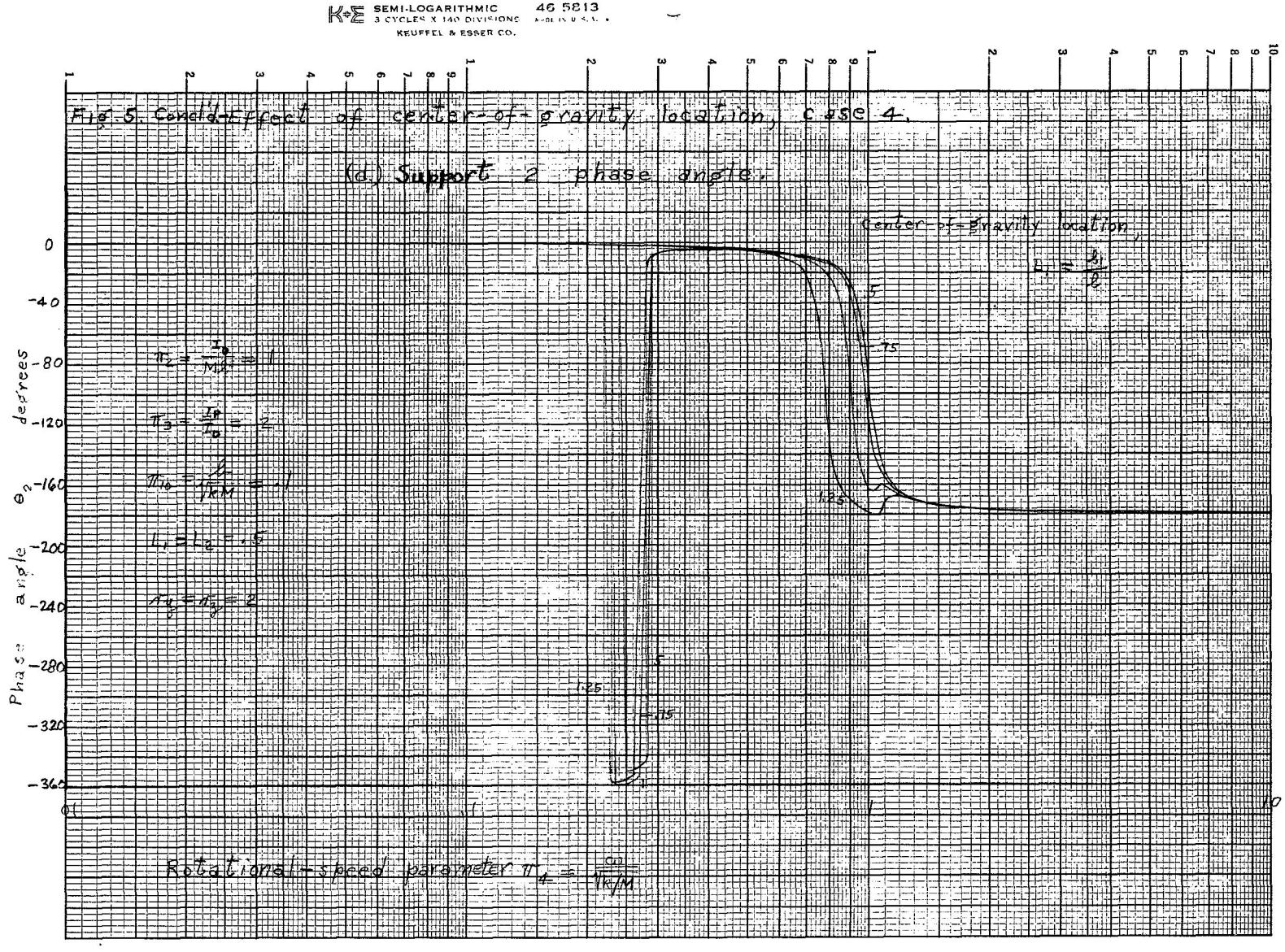
K+E SEMI-LOGARITHMIC 46 5813
3 CYCLES X 140 DIVISIONS
KEUFFEL & ESSER CO.
Fig. 5. Concld-Effect of center-of-gravity location, case 4.
(d.) Support 2 phase angle.
Center-of-gravity location
$\pi_1 = \frac{s}{l}$
.5
.75
1.25
$\pi_2 = \frac{I_0}{M l^2} = 1$
$\pi_3 = \frac{I_p}{I_0} = 2$
$\pi_{10} = \frac{l}{\sqrt{k/M}} = 1$
$l_1 = l_2 = .5$
$\pi_9 = \pi_3 = 2$
Phase angle θ_2 degrees
0
-40
-80
-120
-160
-200
-240
-280
-320
-360
Rotational-speed parameter $\pi_4 = \frac{\omega}{\sqrt{k/M}}$

Figure 6 - Effect of damping parameter for center of gravity at bearing 2, case 5.

(a) Support 1 deflection amplification.

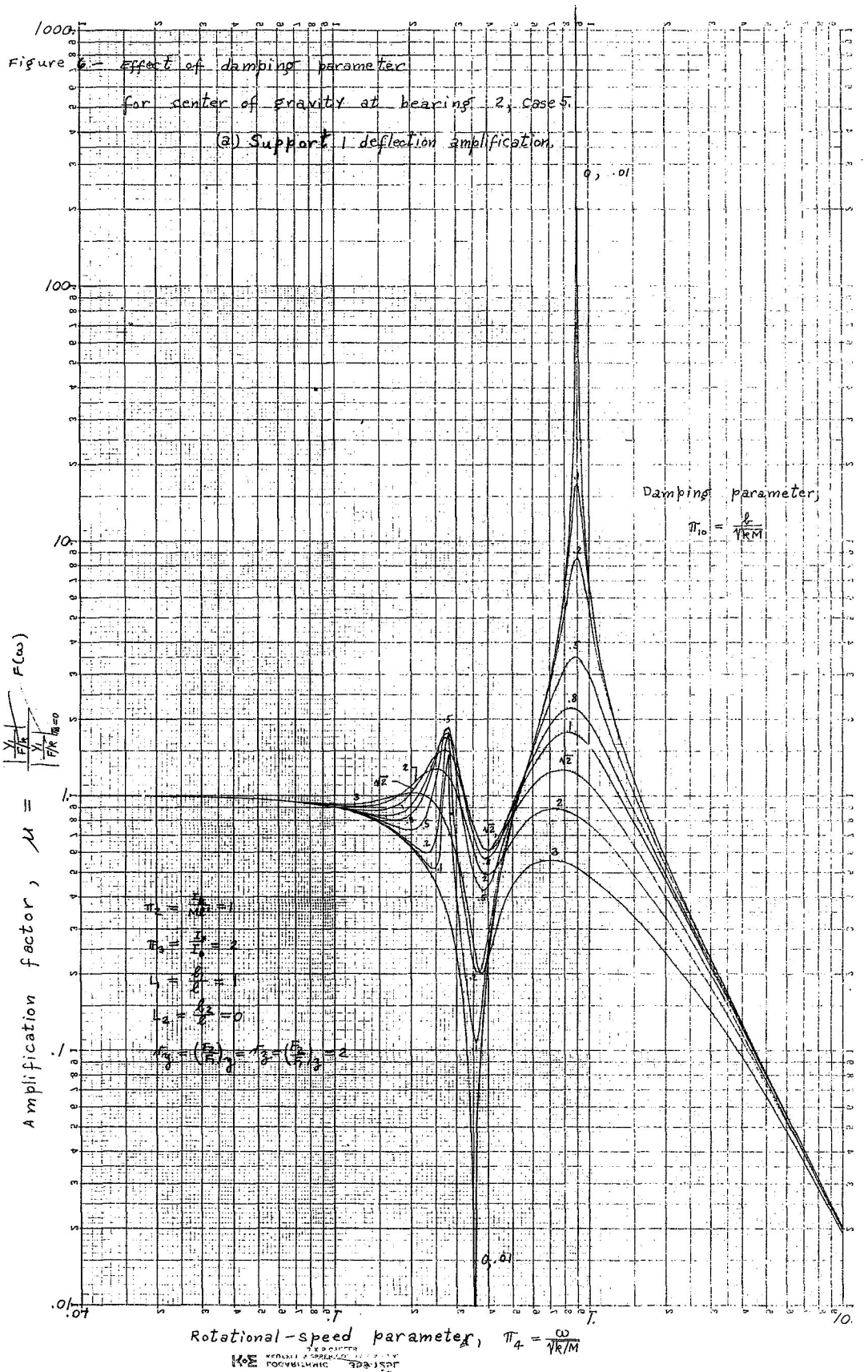

E-6504

Fig 6 Concluded. Effect of damping parameter for center of gravity at bearing 2, case 5.

(b) Support 2 deflection amplification.

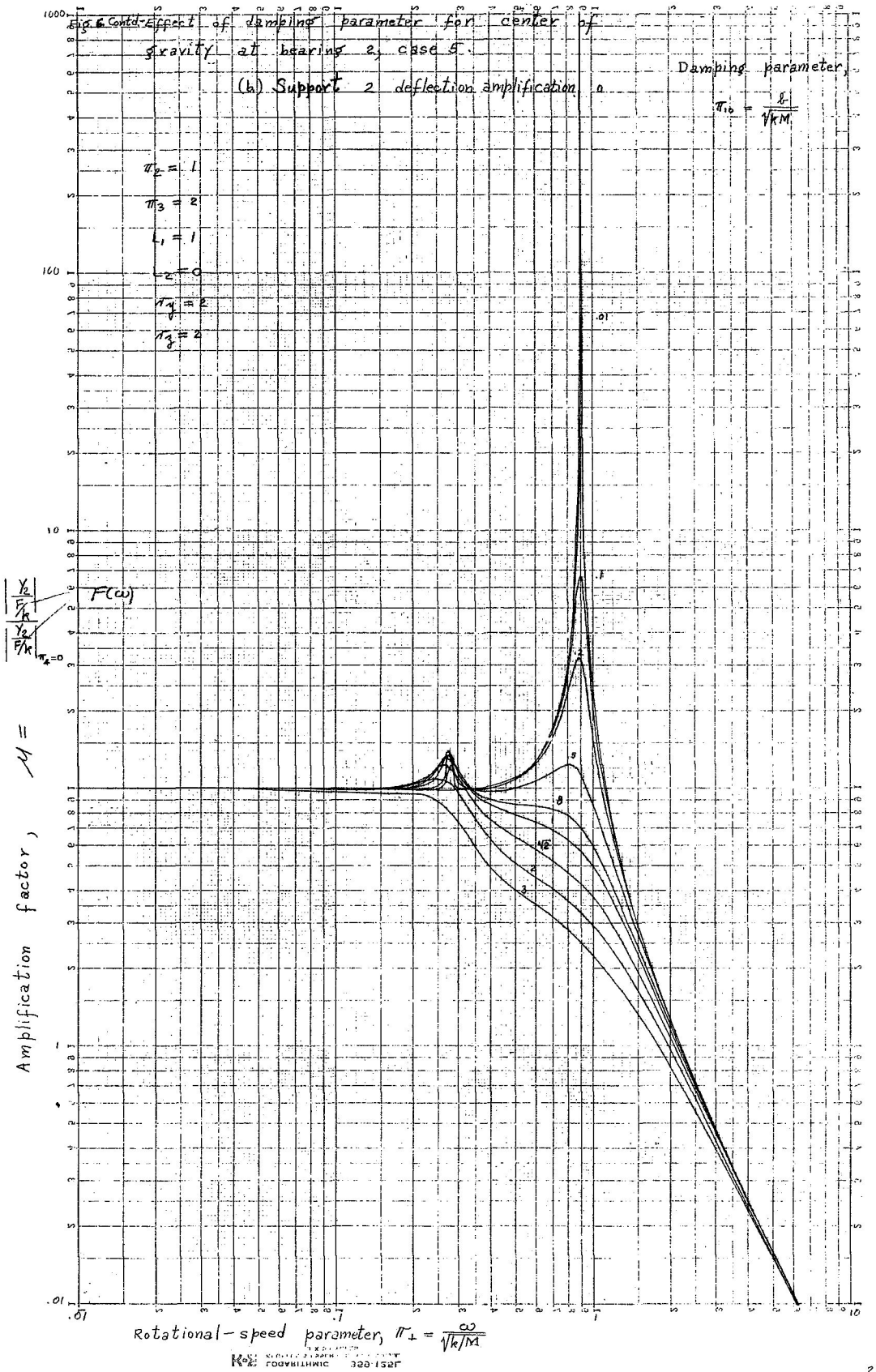

27 MAY

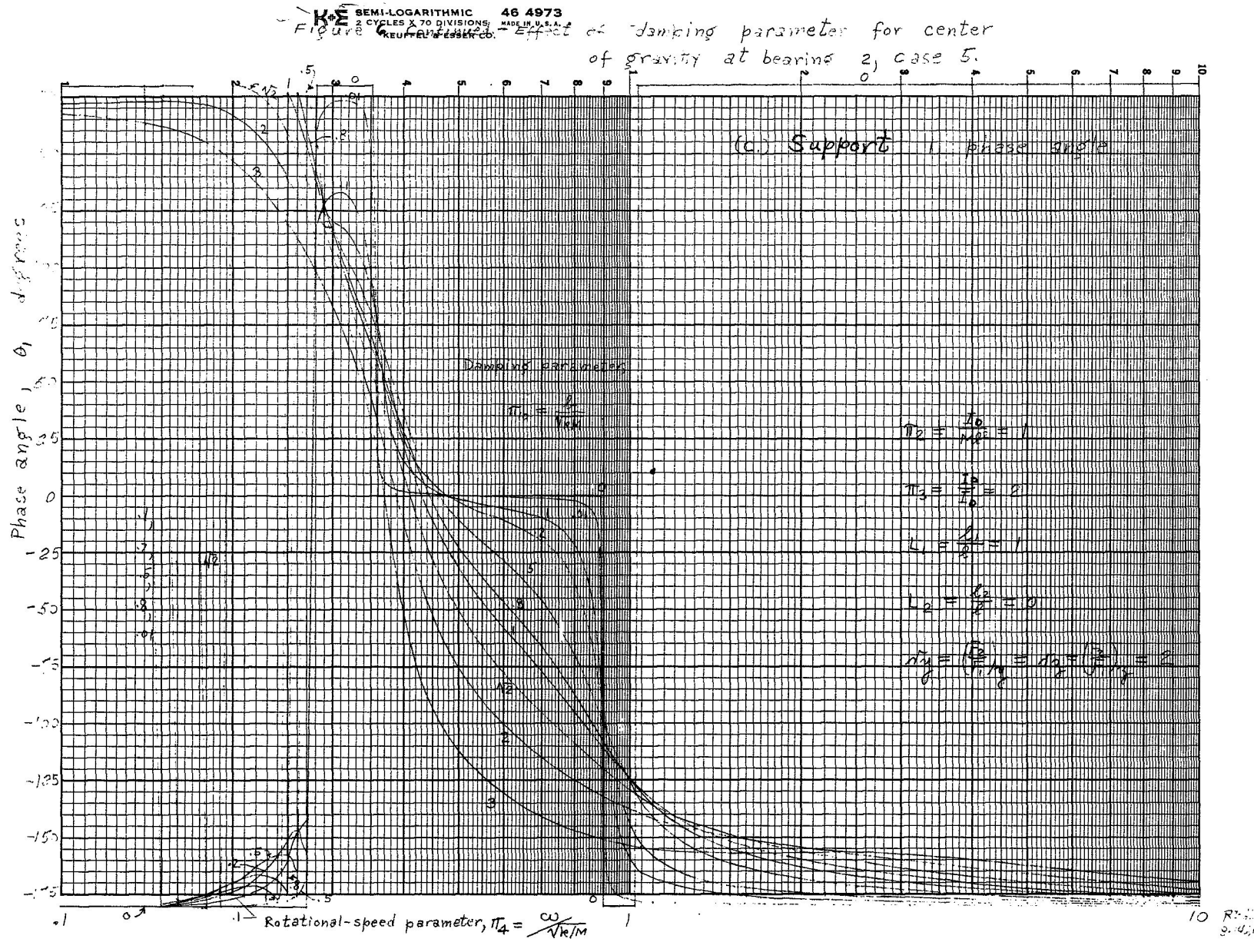
K&E SEMI-LOGARITHMIC 46 4973
2 CYCLES X 70 DIVISIONS MADE IN U.S.A.
KEUFFEL & ESSER CO.
Figure 6.- Effect of damping parameter for center of gravity at bearing 2, case 5.
(c.) Support 1 phase angle
Phase angle, θ_1, degrees
Damping parameter $\pi_{D_2} = \frac{\beta}{\sqrt{k_2 M}}$
$\pi_2 = \frac{I_D}{M\ell^2} = 1$
$\pi_3 = \frac{I_D}{I_D} = 0$
$L_1 = \frac{\ell_1}{\ell} = 1$
$L_2 = \frac{\ell_2}{\ell} = 0$
$\pi_{y_2} = \left(\frac{\ell_2}{\rho_1}\right)_{k_2} \equiv \pi_{D_2} = \left(\frac{\beta}{\sqrt{k_2 M}}\right)_{k_2} = 2$
Rotational-speed parameter, $\pi_4 = \frac{\omega}{\sqrt{k_2/M}}$

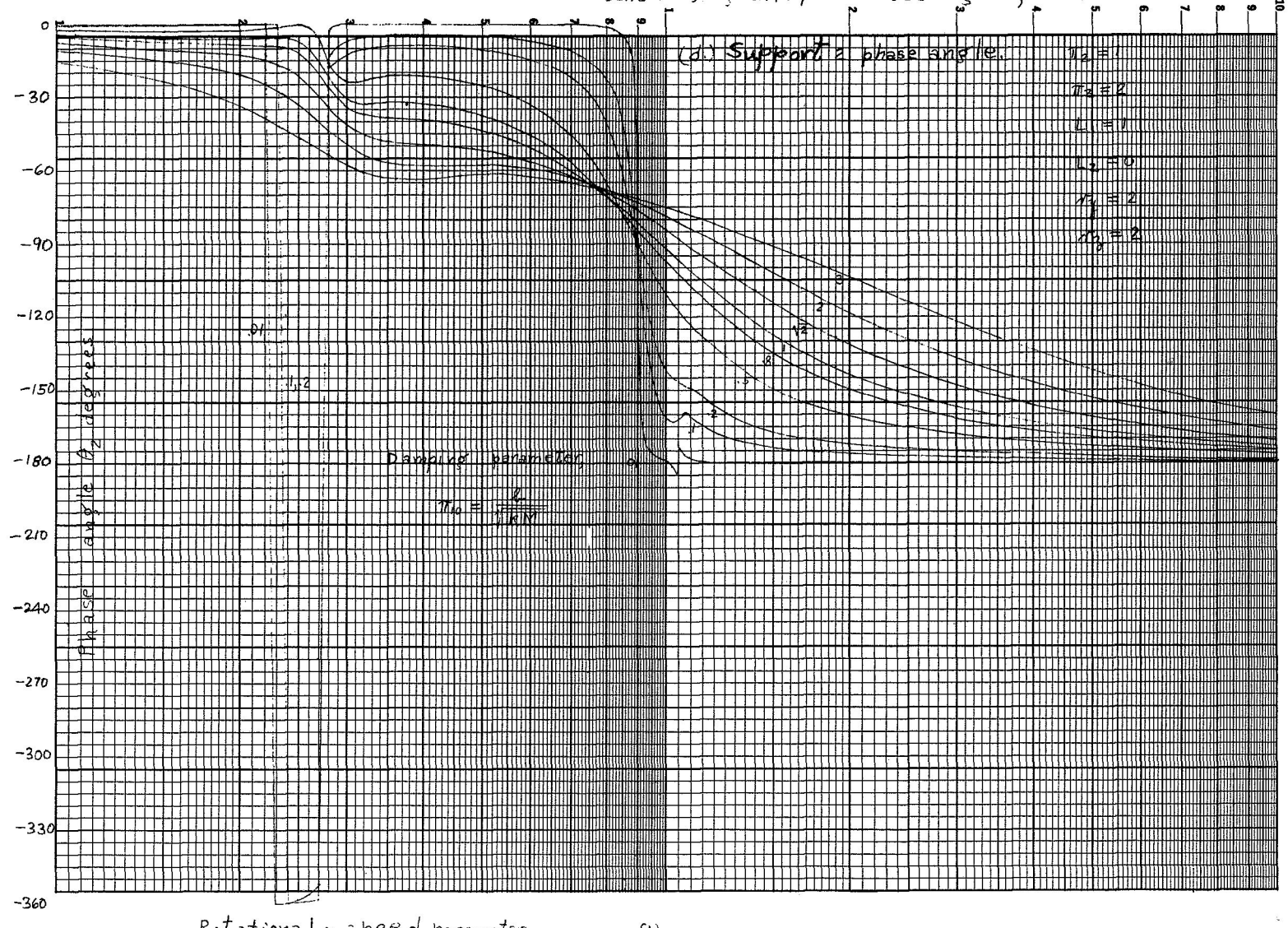

Figure 6. - Concluded. Effect of damping parameter for center of gravity at bearing 2, case 5.

28 MAY 57

Figure 7-Effect of moment-of-inertia ratio for $r_y = r_z = 2$, case 6.

(a) Support 1 deflection amplification.

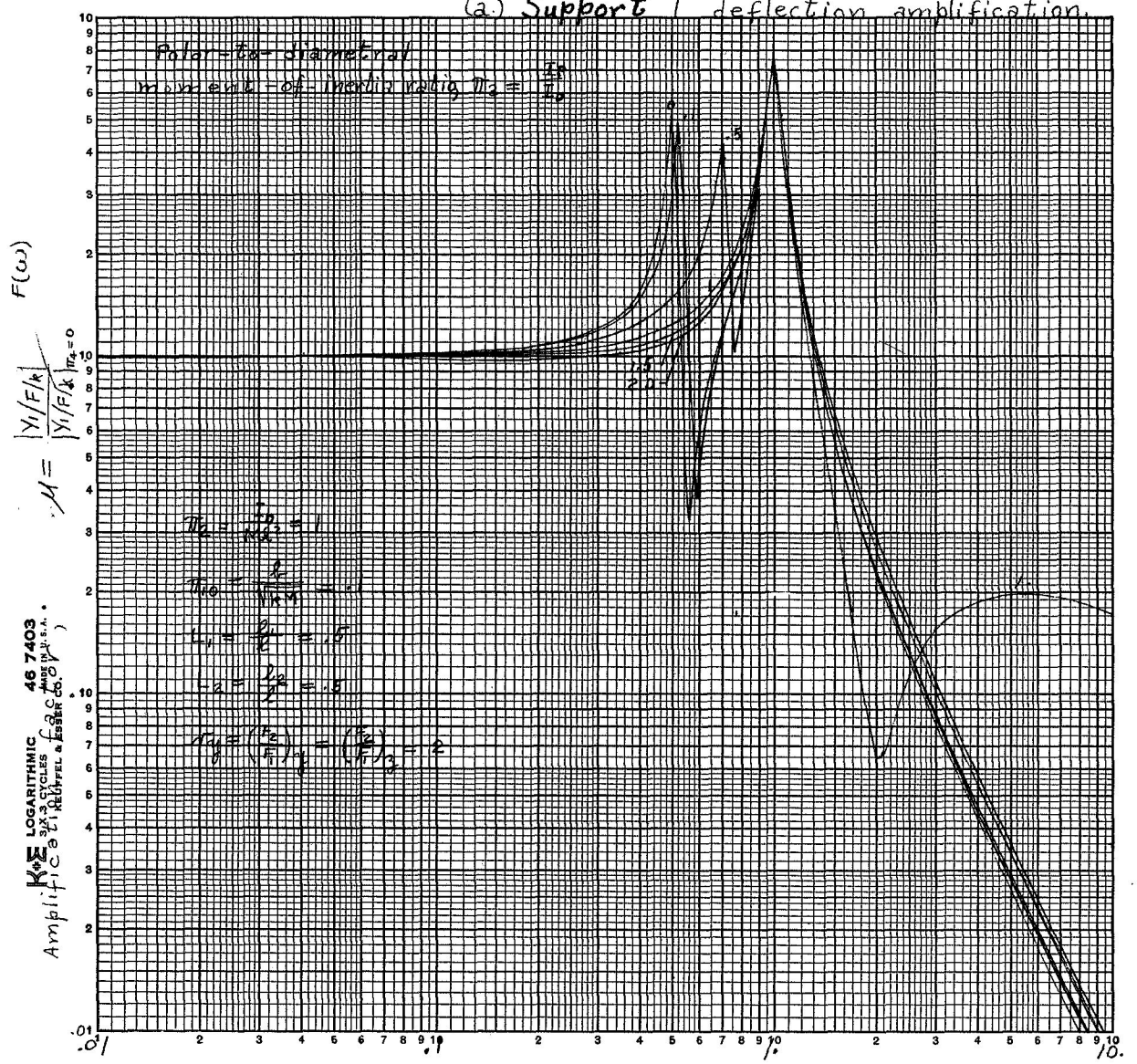

Rotational-speed parameter, $\pi_4 = \frac{\omega}{\sqrt{k/M}}$

7701

RC 6.0
7-28-69

E-6504

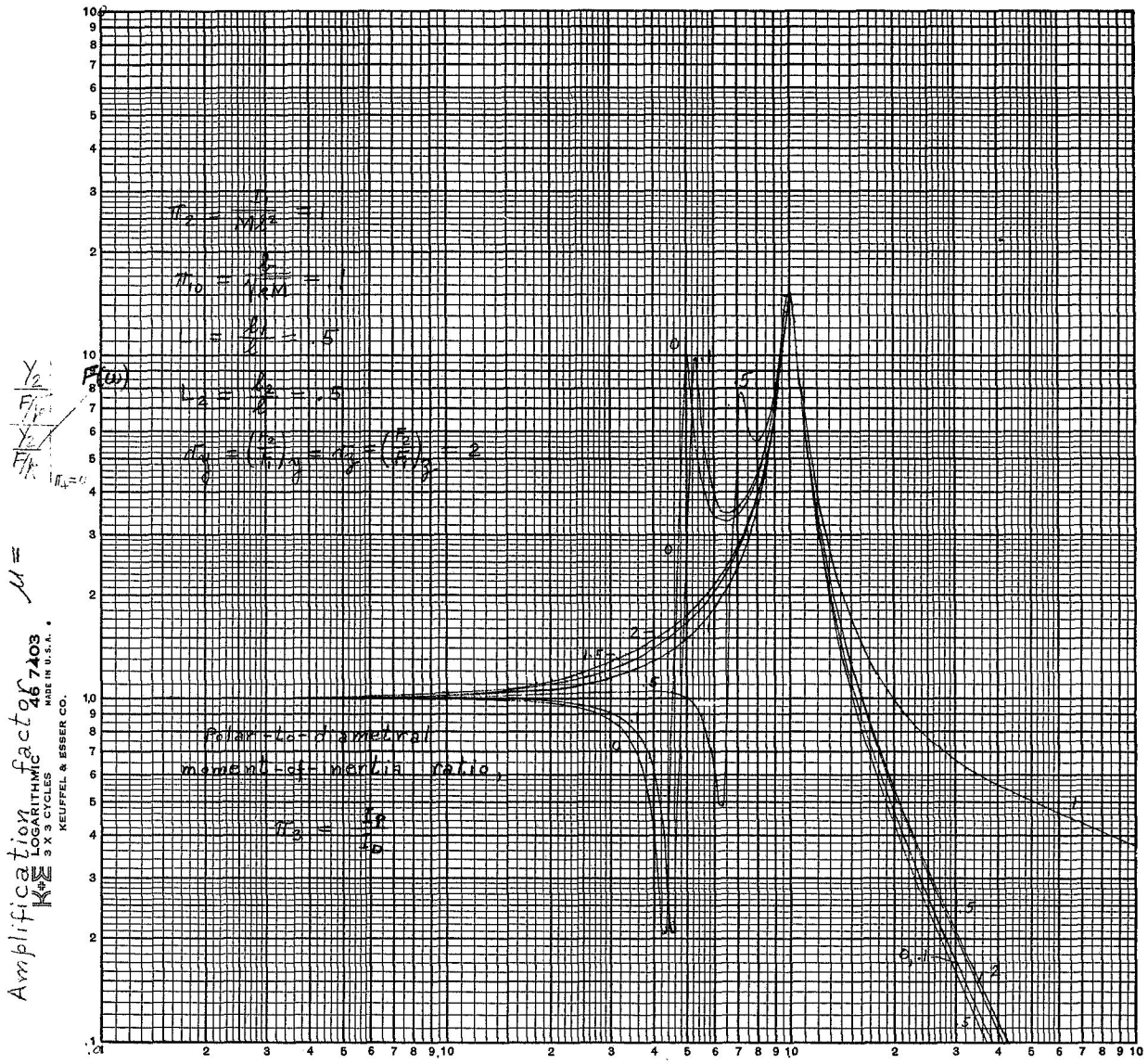

Fig. 7. Cont'd. Effect of moment-of-inertia ratio for $r_y = r_z = 2$, case 6.
(b.) Support 2 deflection amplification.

28 MAY 59

Figure 7. Continued. Effect of moment-of- inertia ratio for $r_y = r_z = 2$, case 6.

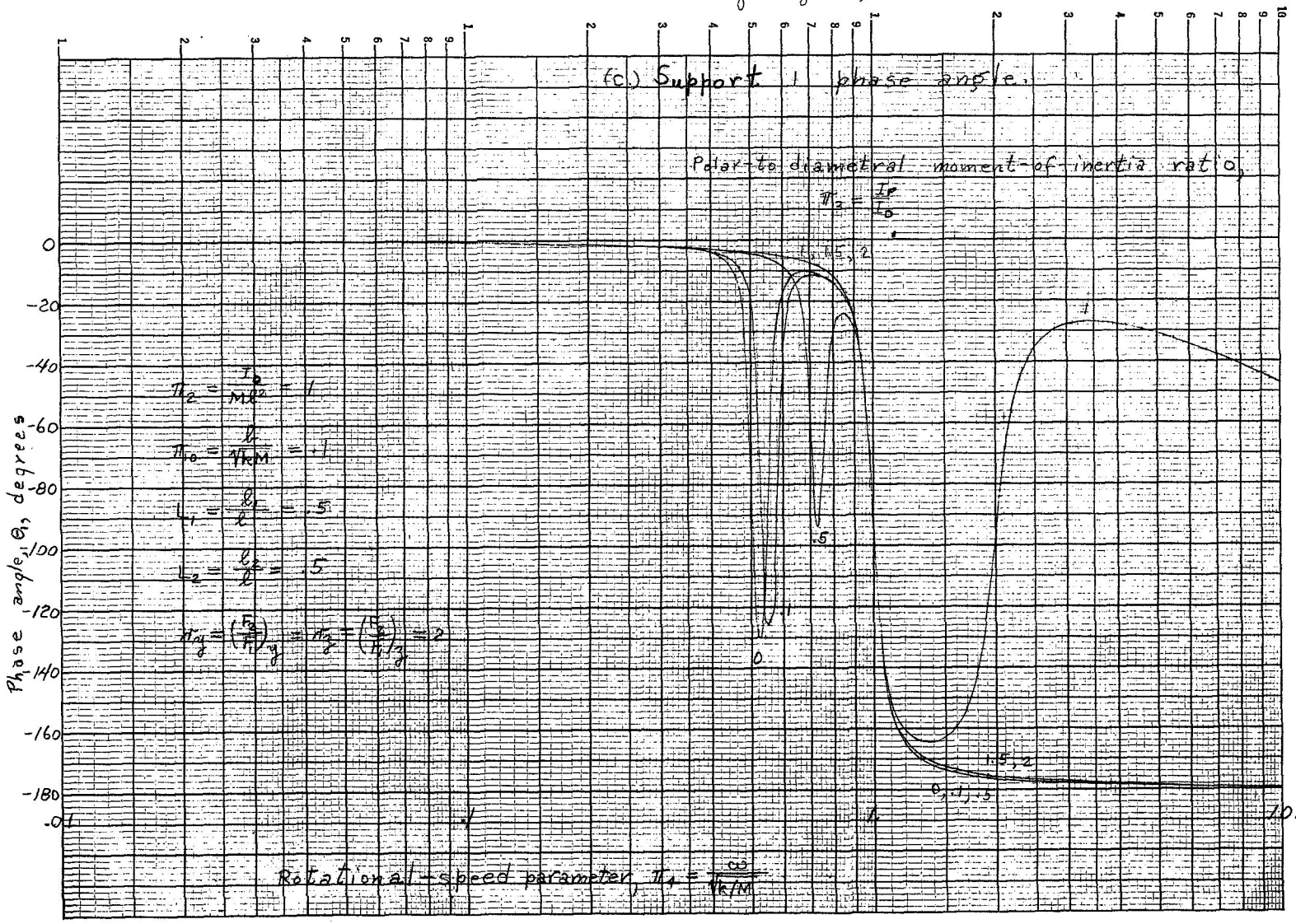

RC/dh
8-1-69

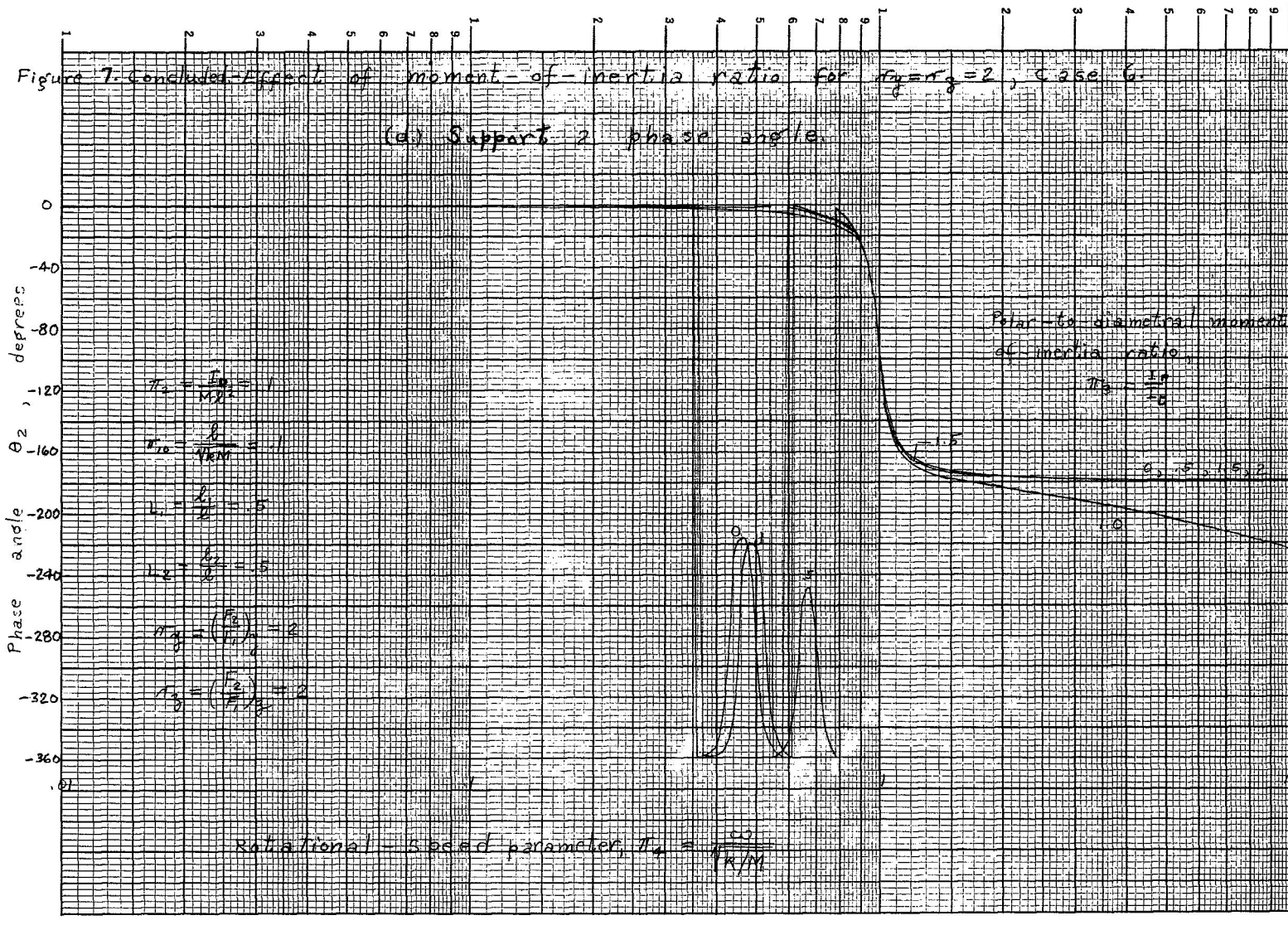
Figure 7. Concluded. Effect of moment-of-inertia ratio for $\pi_{I_1} = \pi_{I_2} = 2$, case 6.
(d) Support 2 phase angle.
Phase angle θ_2, degrees
0
-40
-80
-120
-160
-200
-240
-280
-320
-360
.01
1
10
$\pi_2 = \frac{I_{P_2}}{MD^2} = 1$
$\pi_{10} = \frac{l}{\sqrt{I_P M}} = 1$
$L_1 = \frac{l_1}{l} = .5$
$L_2 = \frac{l_2}{l} = .5$
$\pi_{I_1} = \left(\frac{I_2}{I_1}\right)_1 = 2$
$\pi_{I_2} = \left(\frac{I_2}{I_1}\right)_2 = 2$
Polar-to-diametral moment-of-inertia ratio, $\pi_3 = \frac{I_P}{I_d}$
1.5
.5
.2
.1
Rational-speed parameter, $\pi_4 = \frac{\omega}{\sqrt{k/M}}$

28 AUG. 69

Figure 8 - Effect of disk effect for $r_{y_1} = r_{z_1} = 2$, Case 7.

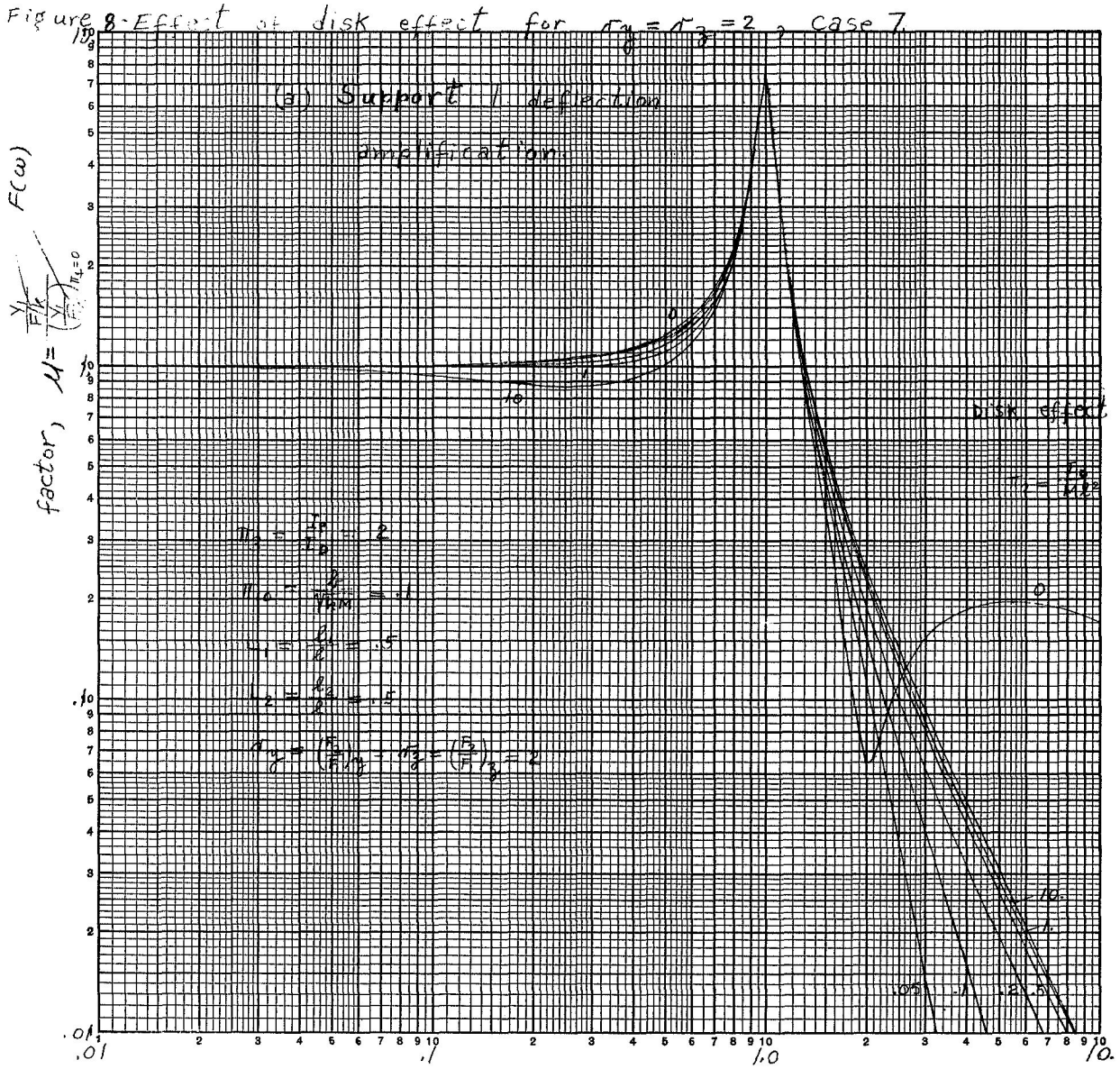

RC/dh
8/1/67

Fig. 8. Continued. Effect of disk effect for $r_y = r_z = 2$, case 7.
(b.) Support 2 deflection amplification.

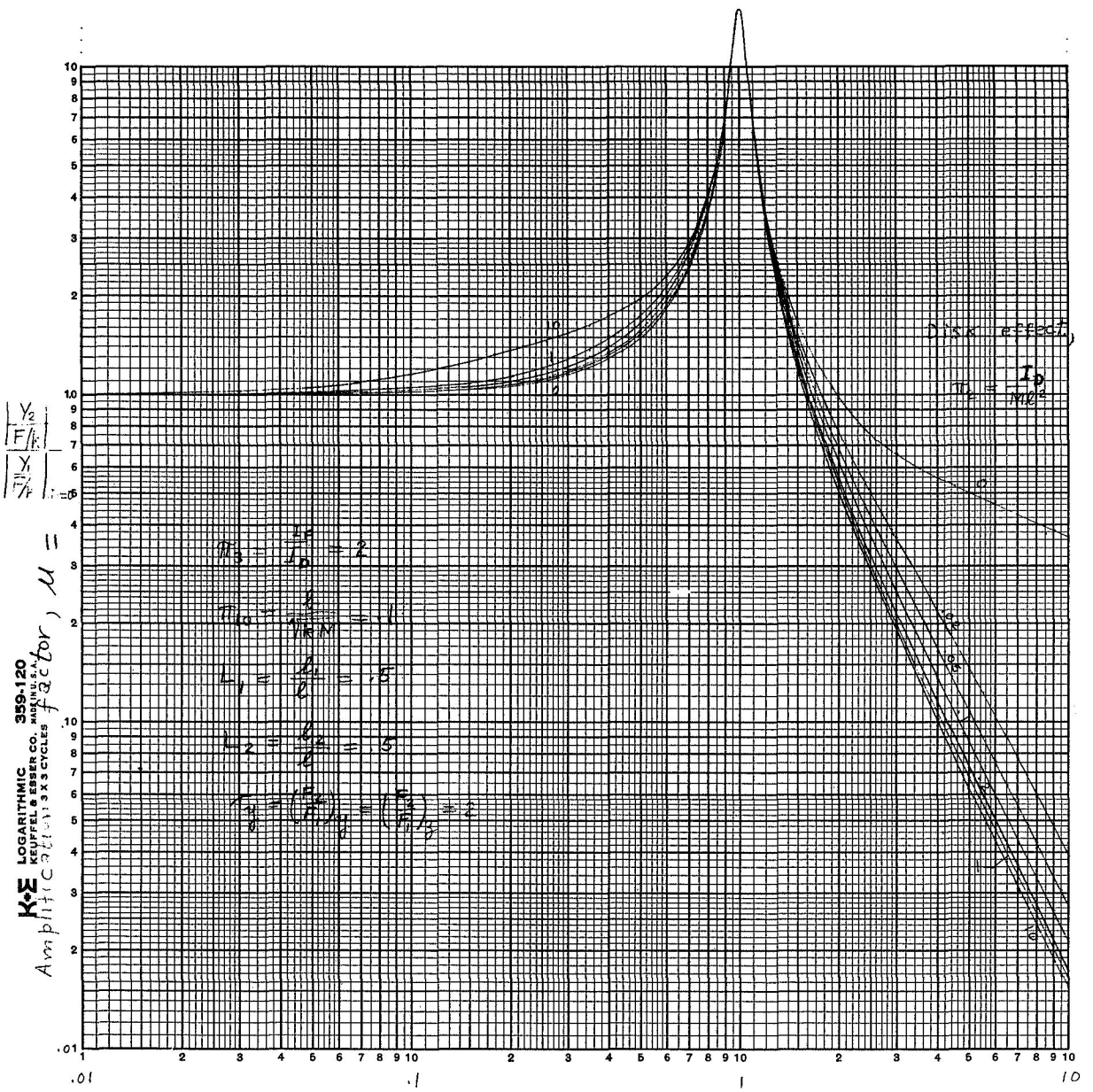

L-6504

11 Sep. 69

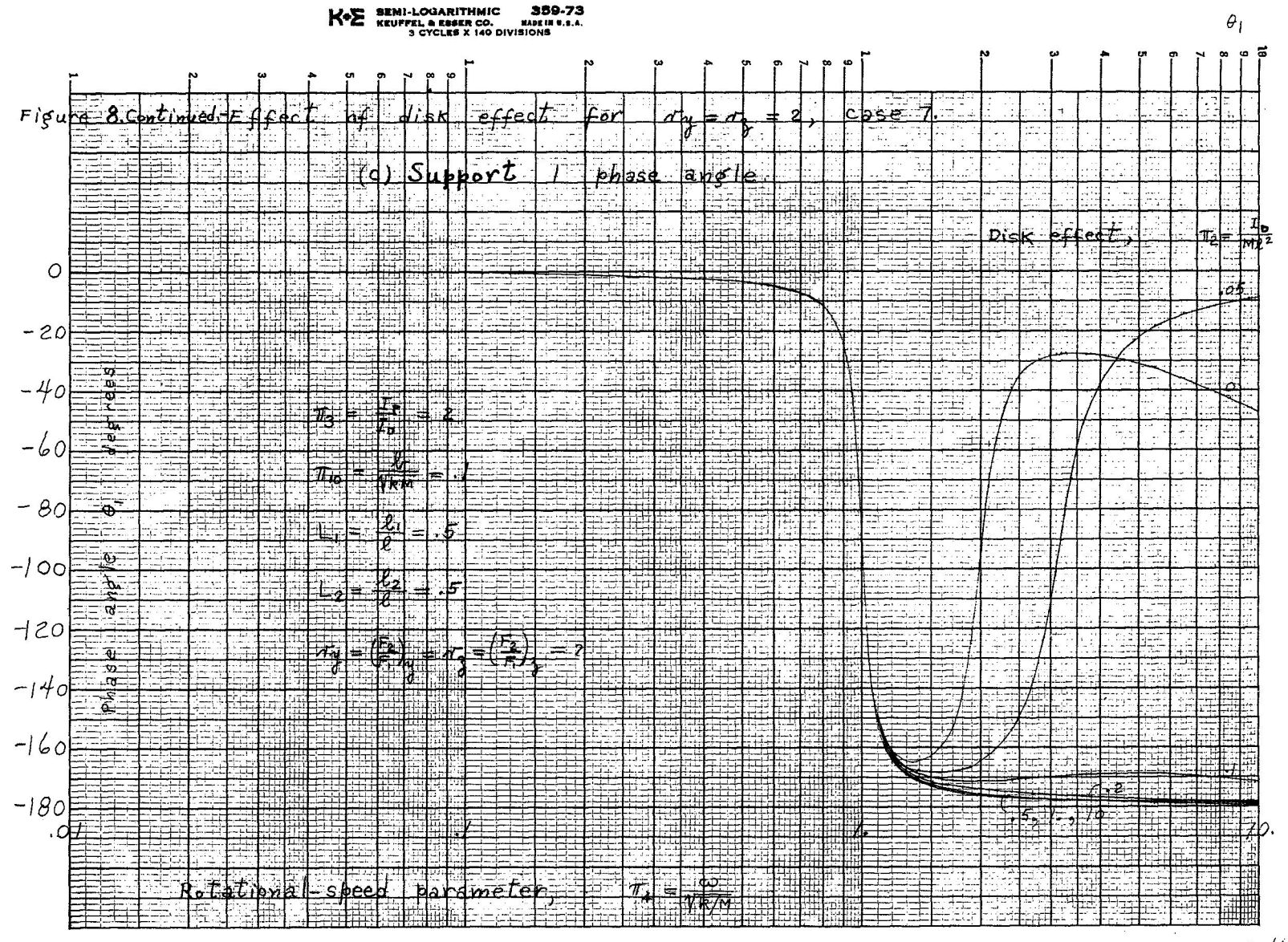
K&E SEMI-LOGARITHMIC 359-73
KEUFFEL & ESSER CO. MADE IN U.S.A.
3 CYCLES X 140 DIVISIONS
θ1
Figure 8.Continued.-Effect of disk effect for π4 = π5 = 2, case 7.
(c) Support 1 phase angle.
Disk effect, π2 = I0/mℓ²
0
-20
-40
-60
-80
-100
-120
-140
-160
-180
Phase angle, -Φ1, degrees
π3 = I0/Iℓ = 2
π10 = k/√kM = .1
L1 = ℓ1/ℓ = .5
L2 = ℓ2/ℓ = .5
π4 = (F2/F1)1 = π5 = (F2/F1)2 = ?
.05
.2
.5
1.
2.
10.
.01
.1
1.
10.
Rotational-speed parameter, π1 = ω/√k/M
RC/dh
8/6/69

Figure 8. Concluded. Effect of disk effect for $r_y = r_z = 2$, case 7.

d. Support 2 phase angle.

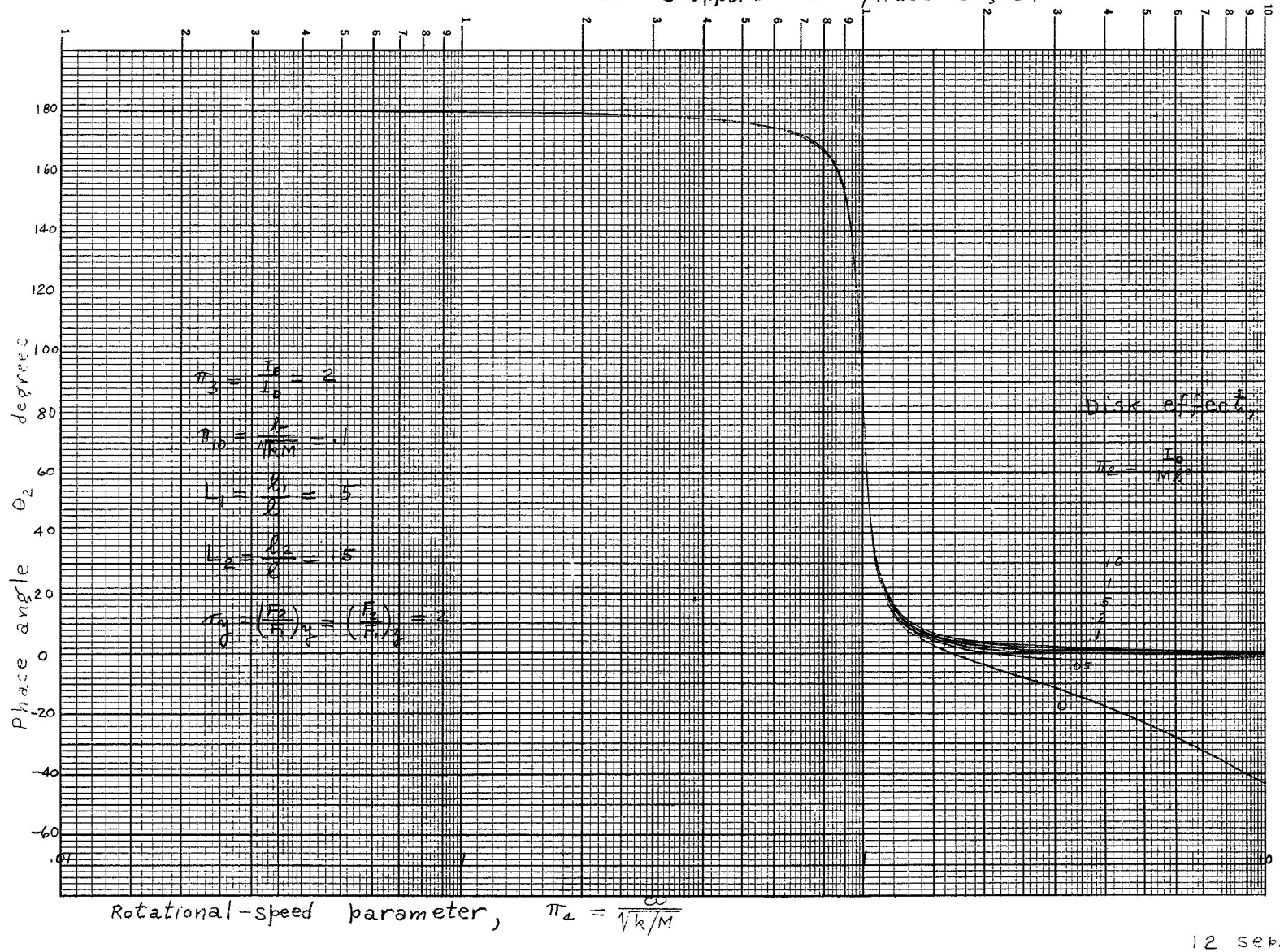

12 Sep. 1969

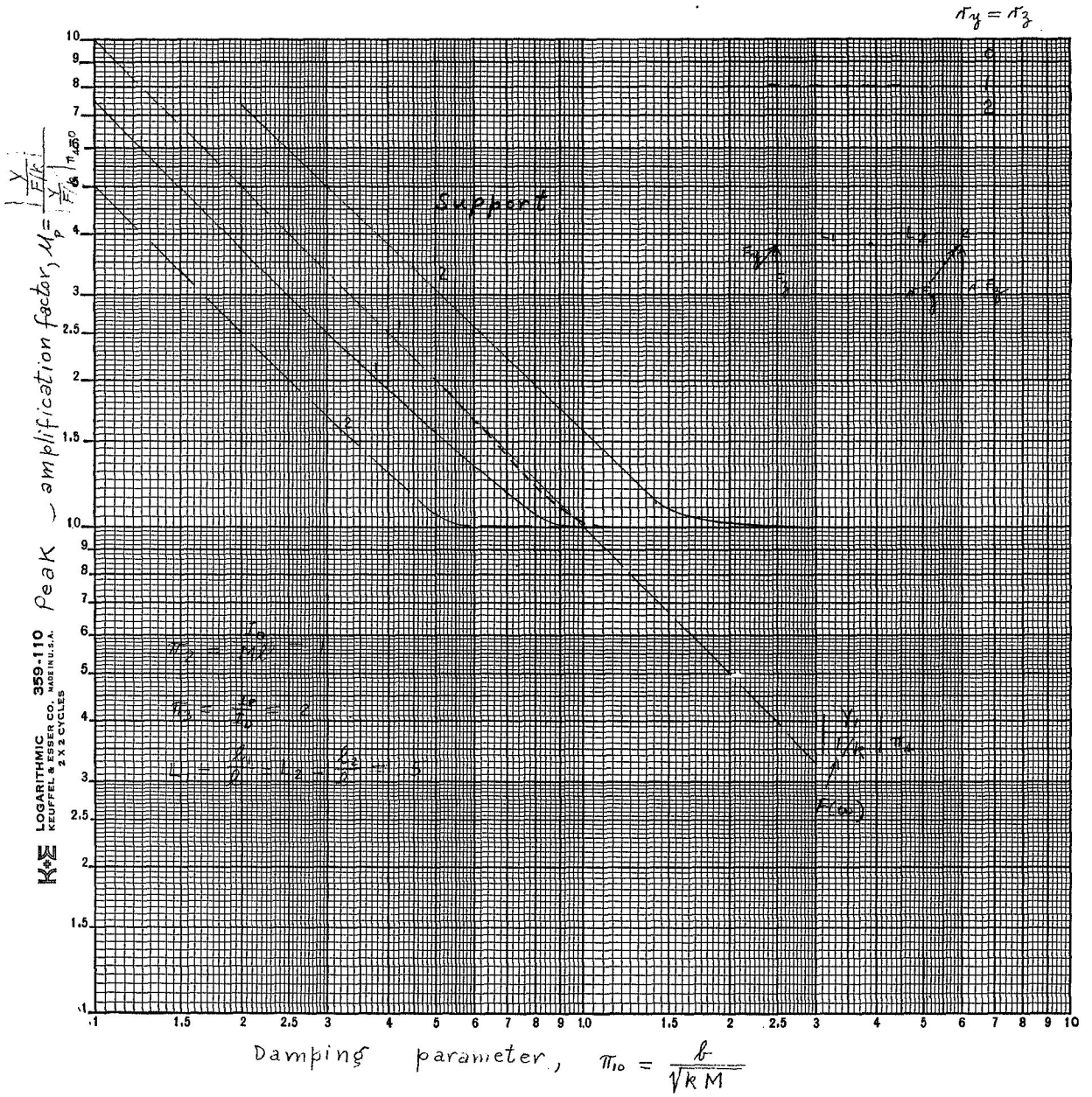

Figure 9.- Effect of damping on peak deflection amplification.

(a.) Variation in force ratio, cases 1, 2, and 3.

16 Sep. 67

Figure 9. Concluded.- Effect of damping on peak deflection amplification.

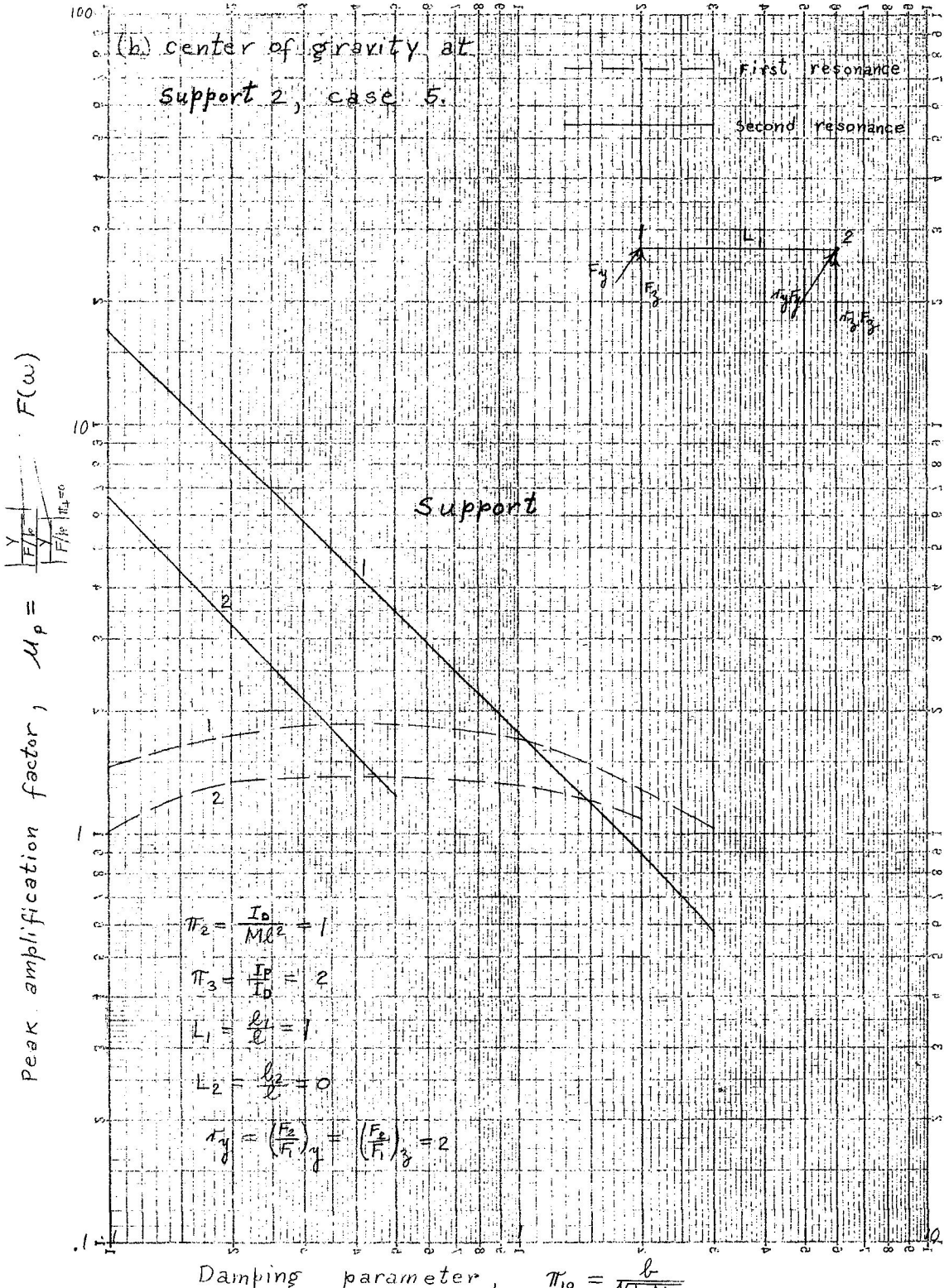

16 Sep. 69

I-6504

Figure 10- Effect of center-of-gravity location on peak deflection amplification, case 4.

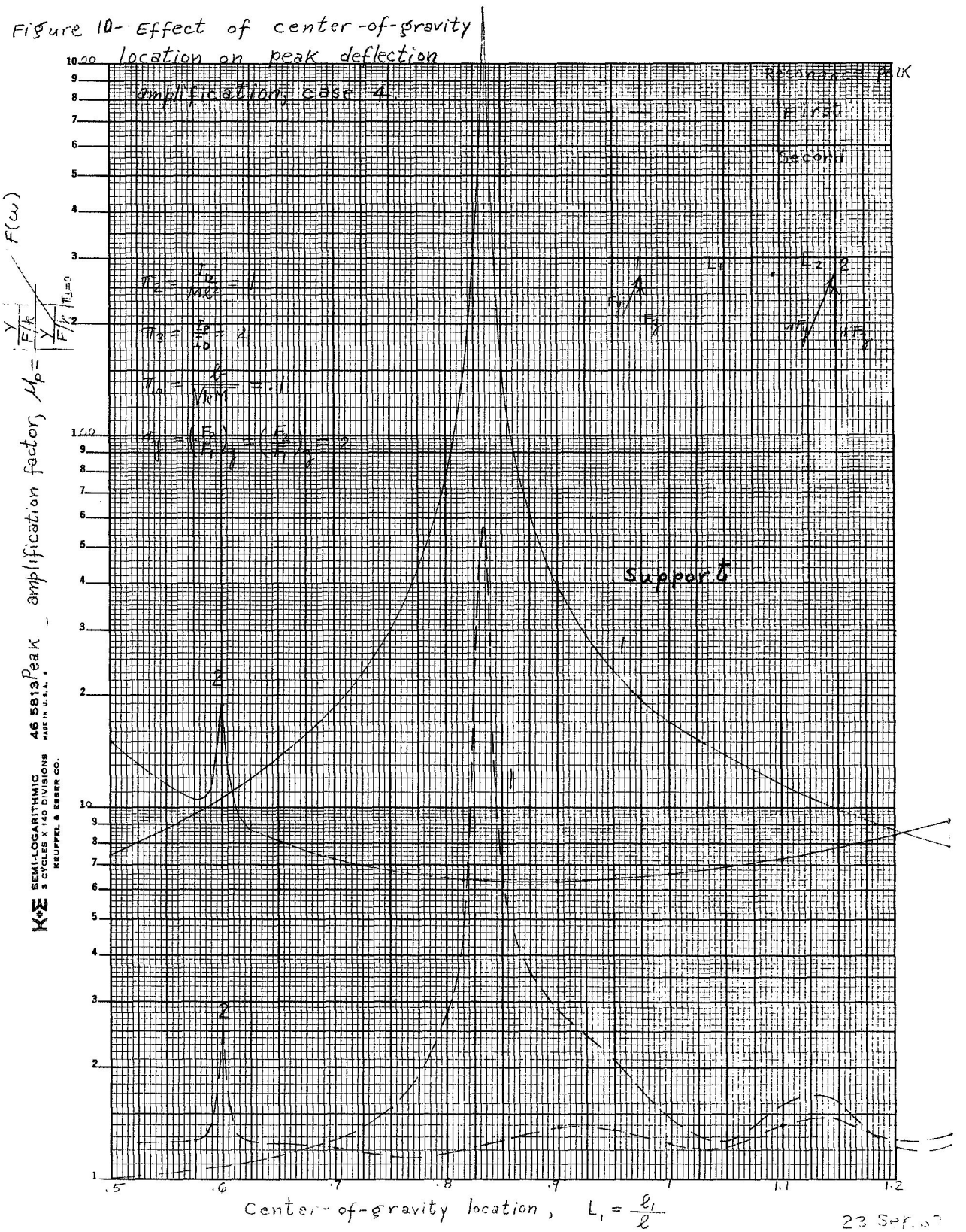

23 Ser...

E-6504

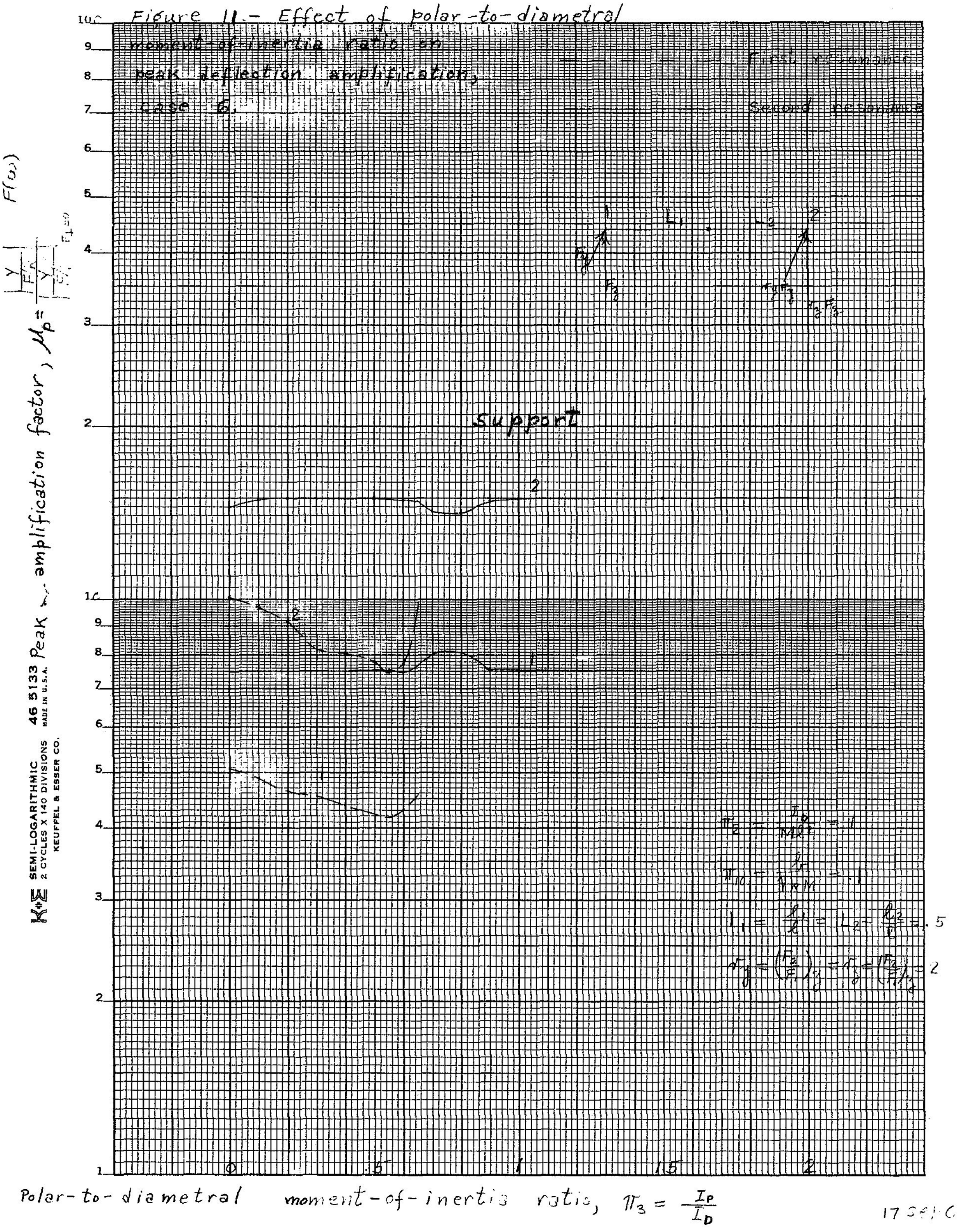

Figure 11.- Effect of polar-to-diametral moment-of-inertia ratio on peak deflection amplification, case 6.

17 961 G

Figure 12.- Effect of support force ratio on peak deflection amplification factor, $\mu_p = \frac{Y}{F/k}$, for center of gravity at midplane, cases 1, 2, and 3.

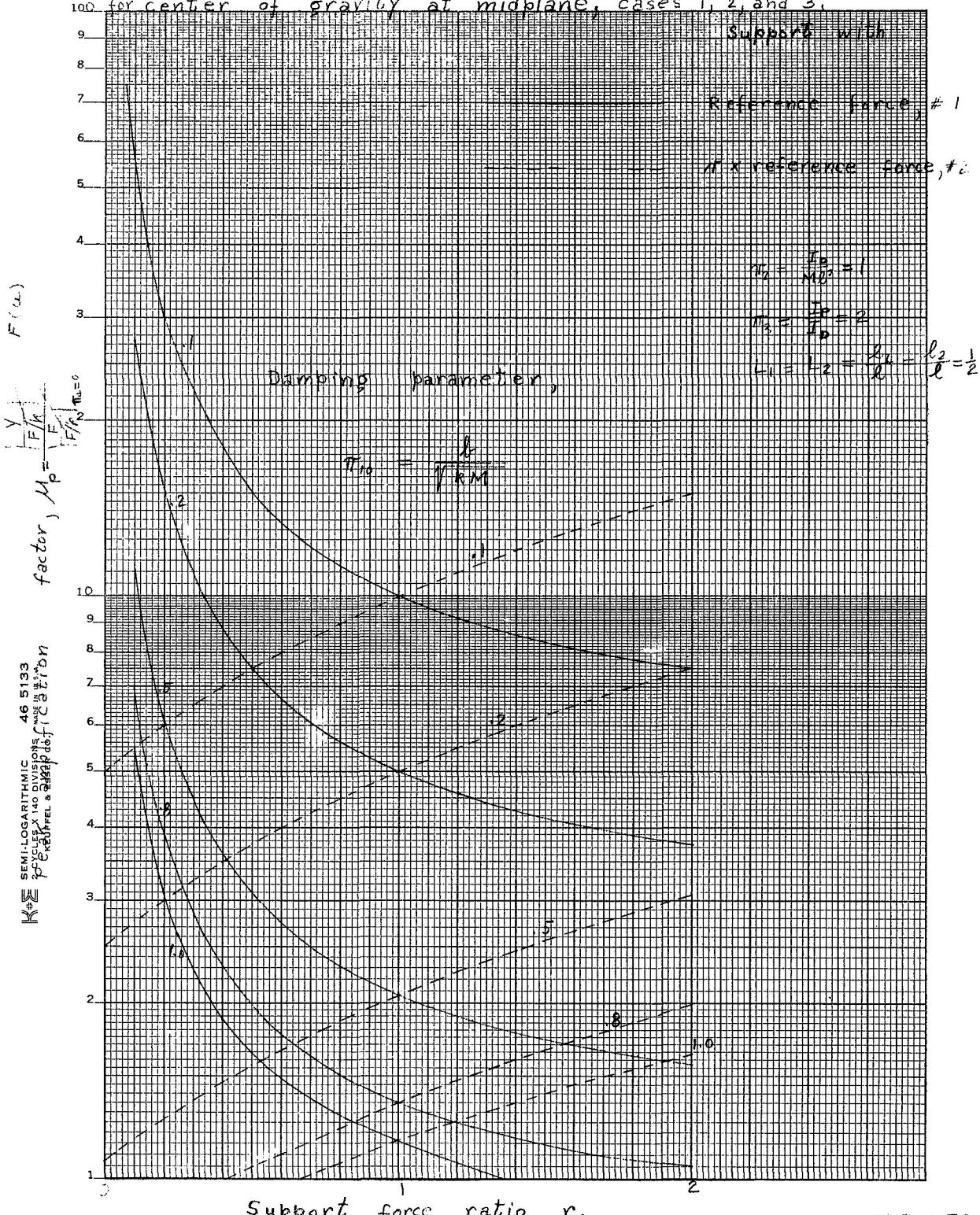

14 Jan. 70